

Galaxy properties in clusters: dependence on the environment and the cluster identification techniques[★]

V. Coenda^{1,2} and H. Muriel^{1,2}

¹ Instituto de Astronomía Teórica y Experimental IATE, CONICET, Laprida 922, X5000BGR, Córdoba, Argentina
e-mail: [vcoenda;hernan]@.mail.oac.uncor.edu

² Observatorio Astronómico, Universidad Nacional de Córdoba, Laprida 854, X5000BGR, Córdoba, Argentina

Received 11 December 2008 / Accepted 10 June 2009

ABSTRACT

Aims. We investigate the dependence of several galaxy properties on the environment and cluster identification techniques.

Methods. We select clusters of galaxies from two catalogues based on the SDSS: the ROSAT-SDSS galaxy cluster survey, which is an X-ray selected cluster sample and the MaxBCG catalogue, in which clusters are optically selected. Based on a volume limited sample of galaxies drawn from the spectroscopic DR5 SDSS, we constructed sub-samples of clusters of galaxies with more than ten members. Scaling relations as well as segregation of galaxy properties as a function of the normalized clustocentric radii are analyzed. The properties of galaxies in clusters are compared with those of field galaxies.

Results. Galaxies in X-ray and MaxBCG selected clusters show similar size-luminosity relations. At equal luminosity, late type galaxies in the field have sizes smaller than cluster galaxies of the same morphological type.

The Faber-Jackson relation for early-type galaxies in clusters is also the same for X-ray selected and MaxBCG clusters. We found clear differences between the dynamical properties of galaxies in clusters, the brightest cluster galaxies (BCG_s) and field galaxies.

Using several criteria to classify galaxies into morphological types, we reproduce the well known morphological segregation. The correlation is up to $r/r_{200} \sim 1$. For the whole range of clustocentric distances, X-ray selected clusters present a higher fraction of early type galaxies than MaxBCG clusters. We also found that bright galaxies preferentially inhabit the cluster centers. Median sizes of galaxies, such as the radius that encloses 50% of Petrosian flux r_{50} , present a behaviour that also depends on the cluster selection criteria. For galaxies in X-ray selected clusters, median values of r_{50} decrease as r/r_{200} goes to zero, whereas the opposite is observed for galaxies in the MaxBCG clusters. These different behaviours are mainly due to early type galaxies.

The results are discussed in terms of the different processes that affect the evolution of galaxies in different environments.

Key words. galaxies: clusters – catalogs – general – galaxies: fundamental parameters – X-rays: galaxies: clusters

1. Introduction

It is well known that galaxies show a wide range of morphologies, which can be appreciated in their properties such as colour, luminosity, size, star formation histories, etc., which imply that galaxies form and evolve through different mechanisms. There have been many studies about the distribution of galaxies with respect to their properties. For example, the luminosity function has been measured from various surveys of galaxies and clusters of galaxies and it is found to be well described by the Schechter function (Schechter 1976; Loveday et al. 1992; Folkes et al. 1999; Madgwick et al. 2002; Cross et al. 2004); the morphological types of galaxies are found to be correlated with the environment, clusters of galaxies being the best example (Dressler 1980; Dressler et al. 1997; Domínguez et al. 2001; Coenda et al. 2006). It is also well known that different galaxy properties are correlated to each other. Galaxy sizes are correlated with the luminosity and morphological type (Andredakis et al. 1995; Möllenhoff & Heidt 2001; Coenda et al. 2005; McIntosh et al. 2005; Trujillo et al. 2006), and have a distribution that may be described by a log-normal function (Syer et al. 1999; de Jong & Lacey 2000; Shen et al. 2003; Ferguson et al. 2004). In order to constrain the galaxy formation models and the study of galaxy properties and

their dependence on environment, we concentrate our studies on several scaling relations and galaxy segregation.

There are different scaling relations between photometric and structural parameters of galaxies, resulting in well known relations. One of the most established empirical scaling relations of disk galaxies is the Tully-Fisher relation (Tully & Fisher 1977), which consist of a correlation between luminosity and rotational velocity. The analogous relation for spheroidal galaxies is the correlation between the velocity dispersion of bulges and luminosity, known as the Faber-Jackson relation: $L \propto \sigma^{\beta}$ (Faber & Jackson 1976). Other scaling relations for spheroidal galaxies are: color-magnitude (Sandage & Visvanathan 1978a,b), color-velocity dispersion (Bernardi et al. 2005), radius-luminosity (Sandage & Perelmuter 1990) and the Kormendy relation, which is a correlation between radius and surface brightness (Kormendy 1977). Some of these properties have been combined to define the so-called *fundamental plane* that relates the velocity dispersion, the effective radius and the luminosity (Djorgovski & Davis 1987; Dressler et al. 1987; Bernardi et al. 2003). These empirical relations are closely related to the physical processes involved in the galaxy formation scenario and, therefore, are a fundamental tool to understand the formation and evolution of galaxies. These relations could depend on the environment where galaxies form and evolve, introducing departures from scatter in the different scaling relations. Several authors have

[★] Appendix A is only available in electronic form at <http://www.aanda.org>

investigated the scaling relations of galaxies in clusters. Ziegler et al. (1999), La Barbera et al. (2004), Bernardi et al. (2007), von der Linden et al. (2007), Liu et al. (2007) and Bildfell et al. (2008). von der Linden et al. (2007) found that brightest cluster galaxies (BCG) have a higher fraction of dark matter and consequently larger radii and higher velocity dispersions than non-BCG galaxies. Malumuth & Kirshner (1981, 1985), Oegerle & Hoessel (1991) and more recently Bernardi et al. (2007) found that BCG have smaller β than the rest of the cluster members. Bernardi et al. (2007) also analyze the dynamical mass ($M_{\text{dyn}} \propto r_{50}\sigma^2$) and found that BCGs show a steeper relation than non-BCG galaxies. The majority of the works mentioned above do not make a suitable comparison with field galaxies, making it very difficult to perform a complete comparison of the scaling relations of galaxies as a function of the environment. More recently, Weinmann et al. (2009) and Guo et al. (2009) analyzed samples of galaxies in groups and found that, at fixed stellar mass, the sizes of central and satellite early type galaxies are similar, while Bernardi (2009), analyzing galaxies in clusters, reported a difference at high luminosities/stellar masses between central and satellite galaxies.

It is well known that different types of galaxies show different spatial distributions (Oemler 1974; Melnick & Sargent 1977; Dressler 1980). These differences can be estimated measuring the radial dependence of the galaxy properties as a function of the clutocentric distance. The segregation of galaxies in clusters has been quantified splitting galaxies according to different properties, with the morphology the property that has been most extensively studied, see for instance Dressler (1980), Whitmore et al. (1993), Domínguez et al. (2001), Biviano et al. (2002), Driver et al. (2003), Coenda et al. (2006). Goto et al. (2002) found that the morphological segregation tends to disappear for clustocentric distances larger than the virial radius. Recently, Martínez et al. (2008) found that $g-r$ color is the property of galaxies that best predict the normalized clutocentric distance of galaxies among a set of galaxy properties. Similarly, Skibba et al. (2008) used the galaxy sample of visual classified morphologies and found that much of the morphology-density relation is due to the relation between colour and density. The works that have studied the segregation in luminosity present some contradictory results. Rood & Turnrose (1968), Yepes et al. (1991), Lobo et al. (1997), Kashikawa et al. (1998), Coenda et al. (2006) found results consistent with a segregation in luminosity. Nevertheless, Noonan (1961), Bahcall (1973) and more recently Pracy et al. (2005) found results consistent with a lack of segregation in luminosity. The segregation of other properties like color, star formation rate, gas content or structural parameters have been much less studied.

The identification of clusters of galaxies is a complex process whose outcome depends on the selection criteria. Popesso et al. (2004) compiled X-ray clusters in the Sloan Digital Sky Survey (SDSS). Using the same survey, Koester et al. (2007b) applied a maxBCG algorithm to identified clusters. This technique is based on the color-magnitude relation of the early type galaxies and the properties of the BCGs. Because we are interested in comparing the galaxy properties of clusters selected with different criteria, the same analysis will be performed on sub-samples of the catalogues compiled by Popesso et al. (2004) and Koester et al. (2007b).

This paper is organised as follows: in Sect. 2 we describe the cluster and galaxy samples; in Sect. 3 we investigate several galaxy scaling relations; in Sect. 4 we analyze the galaxy segregation. We summarise and discuss our results in Sect. 5.

2. The sample

2.1. The cluster sample

We use two catalogues of clusters of galaxies based on the Sloan Digital Sky Survey (York et al. 2000): the ROSAT-SDSS galaxy cluster survey of Popesso et al. (2004, hereafter P04), which is a X-ray selected cluster sample and the MaxBGC Catalogue of Koester et al. (2007b, hereafter K07), which is an optically selected cluster sample.

The ROSAT-SDSS catalogue of Popesso et al. (2004) comprises 114 galaxy clusters detected in the ROSAT All Sky Survey (RASS) lying in the area surveyed by the SDSS by February 2003. This X-ray-selected catalogue includes clusters with masses from $10^{12.5} M_{\odot}$ to $10^{15} M_{\odot}$ in the redshift range $0.002 \leq z \leq 0.45$. This catalogue provides X-ray properties of the clusters derived from the ROSAT data, parameters of the galaxy luminosity function and the luminosity of each cluster computed from SDSS data, and the radial distribution of the projected galaxy density around clusters. Since the X-ray observations provide a robust method for identifying clusters, these clusters constitute a reliable source of information to study galaxy properties and their correlation with the environment.

The optical MaxBGC catalogue provides sky locations, photometric redshift estimates and richness for 13 823 clusters. Details of the selection algorithm and catalogue properties are published in Koester et al. (2007a,b) The MaxBGC selection relies on the observation that the galaxy population of rich clusters is dominated by bright red galaxies tightly clustered in colour (the E/S0 ridgeline). Since these galaxies are old, passively evolving stellar populations, their $g-r$ colours closely reflect their redshifts. The brightest red galaxy, typically located at the peak of the galaxy density, defines the cluster centre. The K07 catalogue comprises galaxy clusters with velocity dispersions $\sigma \geq 400 \text{ km s}^{-1}$ and redshifts $0.1 \leq z \leq 0.3$. Each of these clusters contains between 10 and 190 E/S0 ridgeline galaxies brighter than $0.4L_*$ (i -band), within a scaled radius r_{200} defined as the mean density of 200 times the mean density of the universe. SDSS spectroscopic redshifts are available for at least the brightest galaxy in 39% of the clusters. The sample is up to 85% complete for clusters with masses $\geq 10^{14} M_{\odot}$.

The sub-samples from P04 and K07 considered in this paper comprise galaxy clusters in the redshift range $0.05 < z < 0.14$. The upper limit was taken in order to have a volume limited sample of galaxies with an adequate balance between the number of clusters, the range in absolute magnitude and the number of cluster members. For K07 clusters, we applied a restriction in the richness, selecting clusters with $N_{\text{gal}} \geq 20$ in order to have cluster masses comparable to those in the P04 sample. The sub-samples are labeled as C-P04 and C-K07 respectively. To select cluster members and estimate the physical properties of clusters, we use the main galaxy sample (MGS, Strauss et al. 2002) of the fifth data release (DR5) of SDSS (Adelman-McCarthy et al. 2007) that is complete down to a Petrosian (1976) magnitude $r = 17.77$. At this point, our sub-samples comprise 54 X-ray galaxy clusters from the P04 sample and 612 from the K07 sample. We show in panel (a) of Fig. 1 the spectroscopic redshift distribution of 114 galaxy clusters of the P04 sample (grey solid line), the photometric redshift distribution of 13823 galaxy clusters of the K07 sample (black solid line), the distributions of those K07 clusters with $N_{\text{gal}} \geq 20$ (dotted line) and the distribution of those K07 clusters with spectroscopic redshifts (dashed line). Panel (b) shows the redshift distributions of the selected clusters C-P04 (grey line) and C-K07 (black line). We cross-correlated the catalogues to pick clusters that are included

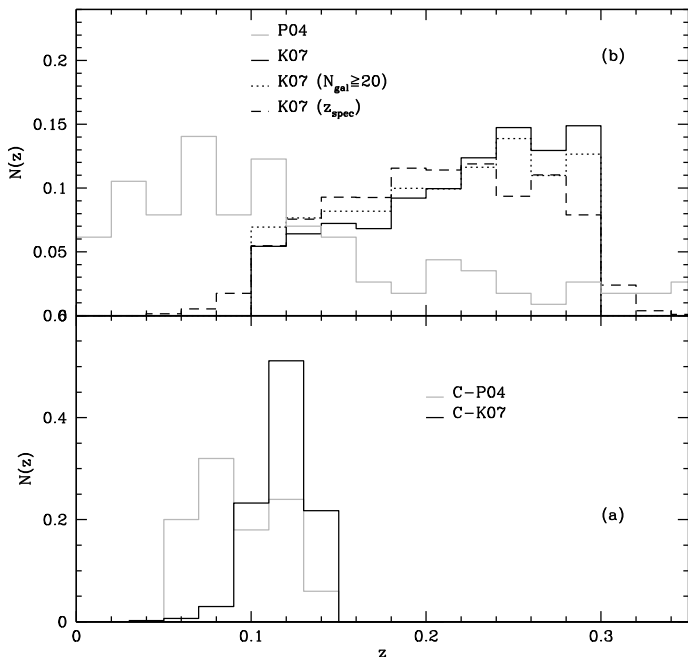


Fig. 1. Panel **a**) shows the spectroscopic redshift distribution of the P04 galaxy clusters (grey solid line), the photometric redshift distribution of the K07 galaxy clusters (black solid line), the distributions of those K07 clusters with $N_{\text{gal}} \geq 20$ (dotted line) and the distribution of those K07 clusters with spectroscopic redshifts (dashed line). Panel **b**) shows the redshift distributions of the selected clusters C-P04 (grey line) and C-K07 (black line).

in both of them. If the projected distance between 2 clusters each belonging to a different catalogue is < 1 Mpc, we consider that they are the same cluster. We found 20 coincidences; in these cases the clusters are only included in the X-ray sub-sample (C-P04).

In order to compute cluster properties such as velocity dispersion, we first identified the cluster members. We use SDSS galaxies from the MGS within a projected radius of 3Mpc centred on the quoted cluster coordinates. From these galaxies we identify cluster members in two steps. First, we use the friends-of-friends (*fof*) algorithm developed by Huchra & Geller (1982) with the percolation linking length values according to Díaz et al. (2005). As a result, we get for each field a list of substructures with at least 10 members identified by *fof*. The second step consists of eyeball examination of the structures detected by *fof*, a comparison between them and the listed cluster position and redshift to determine which coordinates and redshift fit better the observed galaxy over-density. From the redshift distribution of galaxies within $|cz - cz_{\text{cluster}}| \leq 3000 \text{ km s}^{-1}$ we determine the line-of-sight extension of each cluster, i.e., a maximum and a minimum redshift for the cluster. We then consider as cluster members all galaxies in the field that are within that redshift range. The Díaz et al. (2005) technique includes an iterative method that provides precise dynamical centres of the clusters. When these centres differ from those computed by Koester et al. (2007a), we adopted the *fof* values. We found that for $\sim 40\%$ for the clusters, the angular position given by the *fof* is different from the original value, whereas for $\sim 17\%$ of the clusters the redshift derived from the *fof* algorithm is a better match to the observed galaxy redshift distribution than those quoted in the original catalogues. Finally, we excluded from our sample those clusters for which the *fof* redshift value lay outside the redshift range we consider in this paper.

Table 1. Mean values of the cluster physical properties of our cluster samples.

Sample	σ [km s $^{-1}$]	R_{200} [h^{-1} Mpc]	M_{vir} [$h^{-1}M_{\odot}$]	R_{vir} [h^{-1} Mpc]
C-P04-I	715	1.77	7×10^{14}	1.75
C-K07-I	675	1.67	6×10^{14}	1.59

Once the members of each cluster are selected, we compute cluster physical properties we are interested in. We compute the line-of-sight velocity dispersion σ , the virial radius and mass and the r_{200} . The line-of-sight velocity dispersion σ is estimated using methods described by Beers et al. (1990). The bi-weight estimator was applied to clusters with ≥ 15 members, whereas the gapper estimator was applied to poorer clusters. The radius r_{200} was computed using the approximation provided by Carlberg et al. (1997). In a first step, we determined these parameters using all the cluster members within a 3 Mpc projected distance. After this step, we recalculated σ and r_{200} using only galaxies located inside r_{200} . Virial radius and masses were computed following Merchán & Zandivarez (2005). The mean values of these parameters are shown in Table 1, where it can be seen that the sample C-P04 includes on average clusters slightly more massive and larger than the sample C-K07. Figure 2 shows the distributions of cluster physical properties of our samples. The distributions of the main properties of the 20 coincident clusters are similar to those of the parent samples.

Through visual inspection we classified clusters based on their substructure. We only consider in our analysis sub-samples of regular clusters, that we label C-P04-I and C-K07-I, and we exclude systems that have two or more close substructures of similar size in the plane of the sky and/or in the redshift distribution. In order to compute the physical properties in a reasonable way, clusters with fewer than 10 galaxy members within r_{200} are excluded (Girardi et al. 1993). Our final galaxy cluster sample comprises 49 clusters from C-P04-I and 209 from C-K07-I. Our sample of MaxBCG clusters is an order of magnitude smaller than the sample considered by Bernardi (2009), also based on the Koester et al. (2007a) catalogue. This difference is mainly due to our restriction to select clusters with at least ten spectroscopic members in the redshift range $0.05 < z < 0.14$. The sample of Bernardi (2009) includes clusters with redshift up to 0.3 and has, on average, fewer than one spectroscopic early-type satellite galaxy per cluster.

2.2. The galaxy sample

In order to avoid the use of weights and since we are interested in bright galaxies, we have constructed a volume limited samples instead of a flux limited sample. Taking into account the depth of our sample ($z < 0.14$) and the apparent magnitude limit of the Main Galaxy Sample of the SDSS, our sample of galaxies only includes objects with $M_{0.1r} < -21.3$. The C-P04-I sample comprises 786 galaxies, while the C-K07-I sample has 3041 galaxies. Figure 3 shows the redshift distributions of galaxies of our samples, C-P04-I clusters with the grey line and C-K07-I sample with the black line. Galaxy magnitudes used throughout this paper have been corrected for galactic extinction following Schlegel et al. (1998), absolute magnitudes have been computed assuming $\Omega_0 = 0.3$, $\Omega_{\Lambda} = 0.7$ and $H_0 = 70 \text{ h km s}^{-1} \text{ Mpc}^{-1}$ and K -corrected using the method of Blanton et al. (2003) (KCORRECT version 4.1). All magnitudes are in the AB system.

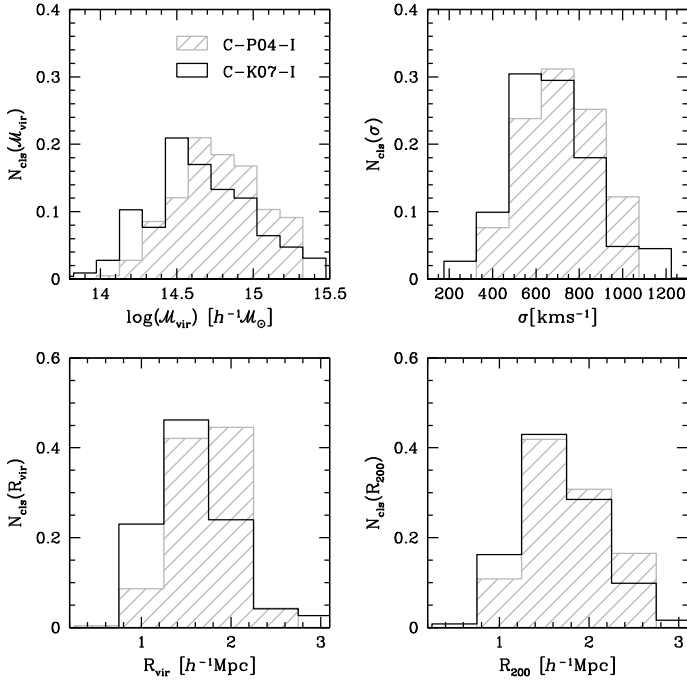


Fig. 2. Distributions of cluster physical properties. The solid grey lines show the C-P04-I sample while the dashed histograms correspond to the C-K07-I sample.

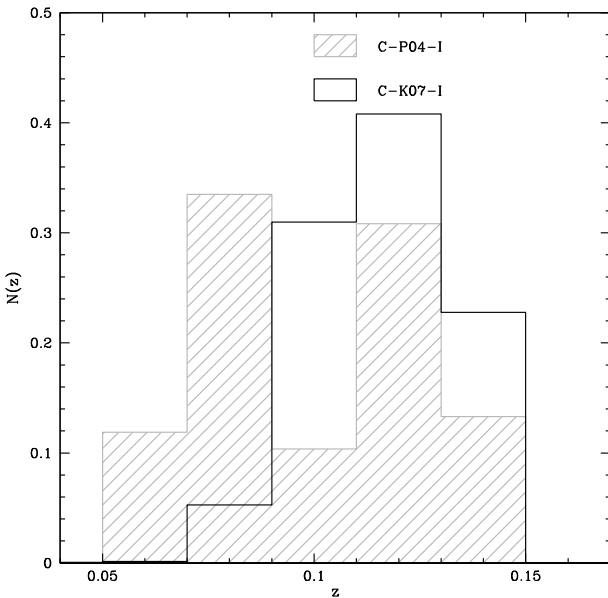


Fig. 3. Redshift distributions of galaxies in our samples. Grey line: C-P04-I sample, black line: C-K07-I sample.

Among the available data for each object in the MGS, we have selected for our analyses parameters that are related to different physical properties of galaxies: luminosity, star formation rate, light distribution inside the galaxies and the dominant stellar populations. In particular, the galaxy parameters we have focused our study on are the Petrosian r -band absolute magnitude $M_{0.1r}$, and the radius that encloses 50% of the Petrosian flux r_{50} . We have chosen Petrosian quantities that are not corrected for the effects of seeing. In order to reduce the effect of the PSF on galaxy sizes, we excluded galaxies with $r_{50} < 2''$, i.e. $0.5''$ greater than the average seeing in SDSS. This is a conservative threshold, since the PSF in SDSS is known quite accurately

(Shen et al. 2003). Hyde & Bernardi (2009) analysed residuals from the size-luminosity relation in the SDSS Petrosian r -band in different redshift ranges. As expected, they found that the effect of seeing increases as a function of redshift. However, in our redshift range ($0.05 < z < 0.14$), these residuals are close to 0.

Our sample consists of bright galaxies in crowded fields where SDSS reductions tend to overestimate the sky level. This results in underestimates of magnitudes and half-light radius for large half-light radii galaxies (Adelman-McCarthy et al. 2008; Bernardi et al. 2007; Hyde & Bernardi 2009). In order to correct the magnitudes and sizes by sky level, we have fitted curves to SDSS simulations (DR6 documentation) and we used these fits to correct the SDSS reductions. Briefly, SDSS quantified the sky effect by adding simulated galaxies (with exponential or de Vaucouleurs) profiles to SDSS images. The simulated galaxies ranged from apparent magnitude $r = 12$ to $r = 19$ in half-magnitude steps, with a one-to-one mapping from r to Sérsic half-light radius (Sérsic 1963, 1968) determined using the mean observed relation between these quantities for MGS with exponential and de Vaucouleurs profiles. Axis ratios of 0.5 and 1 were used, with random position angle for the non-circular simulated galaxies. They found a difference between the input magnitude and the model magnitude returned by the SDSS photometric pipeline, as a function of magnitude. Their results are consistent with a separate analysis performed by Hyde & Bernardi (2009). Finally, we have estimated the rest-frame radius r_{50} in r -band interpolating the observed radii in the adjacent i -band as in Hyde & Bernardi (2009).

Since the aim of this work is to analyze scaling relations and segregation of different types of galaxies in clusters and its comparison with field galaxies, we adopt several criteria to classify galaxies. Shimasaku et al. (2001) found that the concentration index shows a strong correlation with morphological type. These authors conclude that C is perhaps the best parameter to classify the morphology of galaxies. They also found that galaxies with $R_{50} < 2''$ show a weaker correlation between C and the morphological type. To separate galaxies into early and late types, we use the r -band concentration index defined as the ratio between the radii that enclose 90% and 50% of the Petrosian flux, $C = r_{90}/r_{50}$. Typically, early-type galaxies have $C > 2.5$, while for late-types $C < 2.5$ (Strateva et al. 2001). We also use the color to discriminate between early and late type galaxies. The corresponding threshold is $^{0.1}(g-r) = 0.8 - 0.03(M_r + 20)$ (see Blanton & Berlind 2007). Other indicator of galaxy type is the mono-parametric spectral classification based on the eigen-template expansion of galaxy's spectrum e_{class} . This parameter ranges from about -0.35 for early-type galaxies to 0.5 for late-type galaxies (Yip et al. 2004); the separation is set at $e_{\text{class}} = -0.1$. Finally, we use the Sérsic index n , taken from Blanton et al. (2005a). The distribution of n shows a bimodal distribution (see for instance Ball et al. 2008; and Driver et al. 2006). The n separation is set at 2.5, the value that divides in equal parts the two distributions and corresponds to objects with approximately equal bulge and disk components. In Fig. 4 we show the distributions of galaxy parameters. We can see that clusters of the C-P04-I sample (on average, slightly more massive than C-K07-I) have a higher fraction of red galaxies than those taken from the C-K07-I sample (89% and 85% respectively).

We are also interested in the study of the brightest cluster galaxies and the comparison with early-type galaxies in both clusters and in the field. We identify the spectroscopic brightest cluster galaxy (BCG_s) in our sample. The BCG_s is not necessarily the true BCG due to the following reasons: i) as a

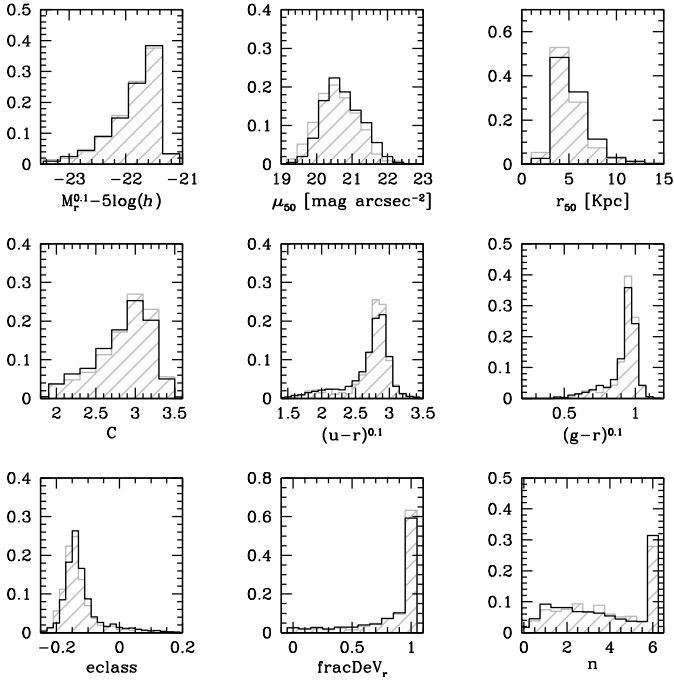


Fig. 4. Distributions of galaxy properties of our samples. Grey line: C-P04-I sample, black line: C-K07-I sample.

consequence of the finite fiber size of the SDSS spectrograph, any two fibers on the same plate need to be spaced at least $55''$ apart. In the case of a fiber collision, objects are selected at random; ii) the MSG is limited at the bright end by the fiber magnitude limits ($r = 14.5$), to avoid saturation and excessive crosstalk in the spectrograph. These two effects together cause the spectroscopic sample to become incomplete.

In Fig. 5 we show the distributions of BCG_s parameters. We find that BCG_s are larger and have lower surface brightness than non- BCG_s , in agreement with von der Linden et al. (2007). In addition, BCG_s have higher velocity dispersion than non- BCG_s . In general, we find that BCG_s have colors, concentration and *eclass* parameters typical of normal early-type galaxies. Despite that BCG_s are usually in the centre of the cluster potential well, we find that the 25% have $r/r_{200} > 0.5$. Nevertheless, it is probable that a fraction of these BCG_s with large r/r_{200} are not the actual BCG. It is also possible that some of the cluster centres are wrong. Finally, we do not find differences between the mean properties of BCG_s in the C-P04-I and C-K07-I samples.

To perform a suitable comparison between cluster and field, we construct a set of comparison samples. These were drawn from MGS and consist of galaxies selected at random having the same redshift distribution as C-P04-I and C-K07-I. This procedure excludes the cluster members. For each cluster catalogue we have two types of samples: i) F-P04-T (52560 galaxies) and F-K07-T (51706 galaxies) that reproduce the corresponding total redshift distribution of galaxies in clusters and ii) F-P04-E, F-P04-L, F-K07-E and F-K07-L that reproduce the redshift distributions and concentration index distributions of the early and late type galaxy population of C-P04-I and C-K07-I, respectively.

3. Scaling relations

3.1. Luminosity-size relation

In this section we use the r -band concentration index C to split galaxies into early and late types, as explained in Sect. 2.2.

In Fig. 6 we show the correlation between luminosity and the Petrosian half-light radius ($r_{50} \propto L^\alpha$). We plot the median values of $\log(r_{50})$ versus $M_r^{0.1}$ for the C-P04-I sample (top panels) and the C-K07-I sample (bottom panels). Error bars were obtained by the bootstrap re-sampling technique. Slopes and zero points in this work correspond to a least-square linear regression. The dotted lines show the 95% confidence bands of the linear regressions. Galaxies in X-ray and MaxBCG selected clusters show similar size-luminosity relations. Early and late type galaxies (red and blue lines respectively) show clear differences, late type galaxies being larger than early types for fixed luminosities. If clusters and field galaxies are compared, we can see in Fig. 6 and Table 2 that late type galaxies in the field (cyan lines) are smaller than galaxies in clusters for a fix luminosity.

For early type galaxies (magenta lines), the differences between field and cluster galaxies are also present, although, they are smaller. The effect is stronger for MaxBCG clusters. Finally, in the common range of luminosity, BCG_s (black lines) tend to be larger and show a steeper $\log(r_{50}) - M_r^{0.1}$ relation than non- BCG_s early type galaxies in clusters. Except for BCG_s , early type galaxies in clusters and in the field show the previously reported curvature in the size-luminosity relation (Bernardi et al. 2007). For these samples of galaxies, linear fits exclude the brightest luminosity bin.

We compare our results of the $r_{50} - M_r^{0.1}$ relation of BCGs with other studies. von der Linden et al. (2007) performed isophotal photometry from the C4 cluster catalogue (Miller et al. 2005) and they found a slope $\alpha = 0.65 \pm 0.02$ for BCGs and $\alpha = 0.63 \pm 0.02$ for a control sample. Liu et al. (2007) derived the luminosity-size relation for 85 BCGs from the same catalogue performing isophotal photometry down to four isophotal limits (22, 23, 24 and 25 mag arcsec $^{-2}$); they found that the luminosity-size relation become steeper as the isophotal limit becomes fainter for both BCGs and control sample galaxies. The slope varies between 0.63 ± 0.04 and 0.88 ± 0.04 for BCGs and between 0.58 ± 0.04 and 0.74 ± 0.04 for the control sample. Although these authors used a similar photometry to von der Linden et al. (2007), the difference in the slopes could be related to the differences in the brightness of the samples. Bernardi et al. (2007) fitted a de Vaucouleurs model to SDSS images from the C4 catalogue and used the half-light radius of their best-fitting models to study the luminosity-size relation. These authors found a slope $\alpha = 0.89$. Lauer et al. (2007) used surface photometry in HST images for 219 early type galaxies and also fitted a de Vaucouleurs model; they found $\alpha = 1.18 \pm 0.06$. Once again, the photometry used in the last two works is similar but the results are very different. Again, a suitable explanation is the difference in the construction of the samples. On the other hands, Guo et al. (2009) used 911 central galaxies from SDSS DR4 group catalogue (Yang et al. 2007). This catalogue is constructed using the New York University value-added galaxy catalog (Blanton et al. 2005b). Guo et al. (2009) fitted a Sérsic luminosity profile to each galaxy using GALFIT (Peng et al. 2002), and found a slope $\alpha = 1.02 \pm 0.03$ over the luminosity range -19 to -24 . For galaxies brighter than -22 , these authors found $\alpha = 0.82 \pm 0.06$. Shen et al. (2003), using spectroscopic SDSS galaxies and also Sérsic luminosity profiles, found $\alpha = 0.65$. Recently, Hyde & Bernardi (2009) used early-type BCGs identified in the SDSS MaxBCGs and C4 catalogs and found $\alpha = 0.6$ for early-type galaxies, while BCGs follow a steeper relation. It should be noted that the slopes resulting from our work are typically shallower than the slopes found in the different works mentioned above. Partially, these differences in slopes could be the result of the different methods used to perform the photometry.

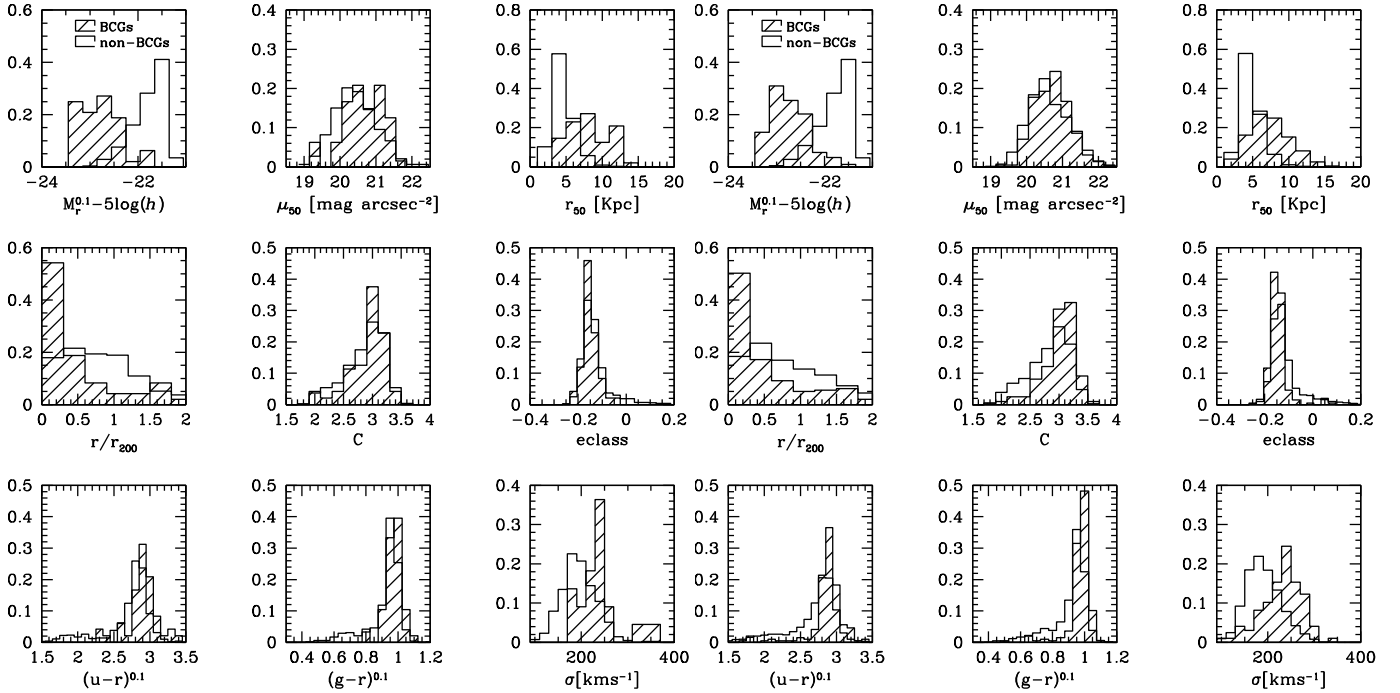


Fig. 5. Distributions of BCG_s (dashed histograms) and $non-BCG_s$ galaxy properties of the samples C-P04-I (left panels) and C-K07-I (right panels).

Table 2. Parameter of the fits $\log(r_{50}) = -0.4\alpha M_r + b$, see Fig. 6.

C-P04-I		
<i>early non-BCGs</i>	<i>BCGs</i>	<i>early field</i>
α	0.48 ± 0.05	0.55 ± 0.08
b	-3.5 ± 0.3	-3.10 ± 0.07
<i>late</i>		<i>late field</i>
α	0.4 ± 0.2	0.278 ± 0.005
b	-3 ± 1	-1.79 ± 0.04
C-K07-I		
<i>early non-BCGs</i>	<i>BCGs</i>	<i>early field</i>
α	0.41 ± 0.02	0.180 ± 0.003
b	-2.9 ± 0.2	-0.91 ± 0.03
<i>late</i>		<i>late field</i>
α	0.40 ± 0.08	0.30 ± 0.01
b	-2.8 ± 0.6	-1.88 ± 0.08

While the works mentioned above used de Vaucouleurs, isophotal or Sérsic models, we used Petrosian magnitudes and sizes. In addition, the sample selection causes variations in the value of the slopes; for example the use or not of spectroscopic data can introduce important differences in the results, as has been demonstrated by Coenda et al. (2006). Beyond the differences in the slopes, it should be noted that BCGs always follow a steeper relation than galaxies in control samples.

3.2. Dynamical relations

It is known that velocity dispersion and luminosity are well correlated for early-type galaxies ($L \propto \sigma^\beta$), a relation known as Faber-Jackson (Faber & Jackson 1976). Figure 7 shows the median values of $\log \sigma$ as function of $M_r^{0.1}$ for early-type galaxies in clusters (red lines), control sample (magenta lines) and BCG_s (black lines). Table 3 gives the parameters of the fits, where we can appreciate that there are no differences between fits

corresponding to both cluster samples. Where we do see a clear difference is between galaxies in clusters (both BCG_s and $non-BCG_s$) and field galaxies, the latter being dynamically cooler (show lower mean velocity dispersions). The $\log \sigma - M_r^{0.1}$ also presents a departure from linearity for the brightest bin, where bright early type galaxies show a lower velocity dispersion than that expected from the linear relation that fits the lower magnitude bins. BCG_s show a $\log \sigma - M_r^{0.1}$ relation flatter than that of non-BCG galaxies. Nevertheless, the mean velocity dispersion that corresponds to the brightest luminosity bin of non-BCG galaxies is consistent with the values expected for BCG_s . Therefore, the flattening of the $\log \sigma - M_r^{0.1}$ relation observed for BCG_s (see also Bernardi et al. 2007) could be a general property of early type galaxies regardless of its nature as the brightest cluster galaxy. Liu et al. (2007) and von der Linden et al. (2007) found that BCGs have a Faber-Jackson relation steeper than that of early-type galaxies. On the contrary, Bernardi et al. (2007) found a shallower relation for BCGs, consistent with our findings.

In Fig. 7 we found that early-type and BCG_s galaxies have, on average, the same velocity dispersions at a given luminosity. We also found that BCG_s have larger sizes than early type galaxies. Therefore, a different trend of dynamical masses as a function of luminosity between these two types of galaxies should be expected. In Fig. 8 we show the median value of $\log(r_{50}\sigma^2)$ as a function of the luminosity for early-types, BGG_s and control-sample galaxies. Again, the brightest bins show a departure from linearity and were excluded from the linear fits. For the three samples we plot a linear regression that confirm that BCG_s have, on average, higher dynamical masses than early-type galaxies of the same magnitude (the fitting parameters are given in Table 4). It should be noted that these differences are more significant for MaxBCG clusters (C-K07-I) than for X-ray clusters (C-P04-I). Field galaxies in control samples show lower dynamical masses than non-BCGs in clusters.

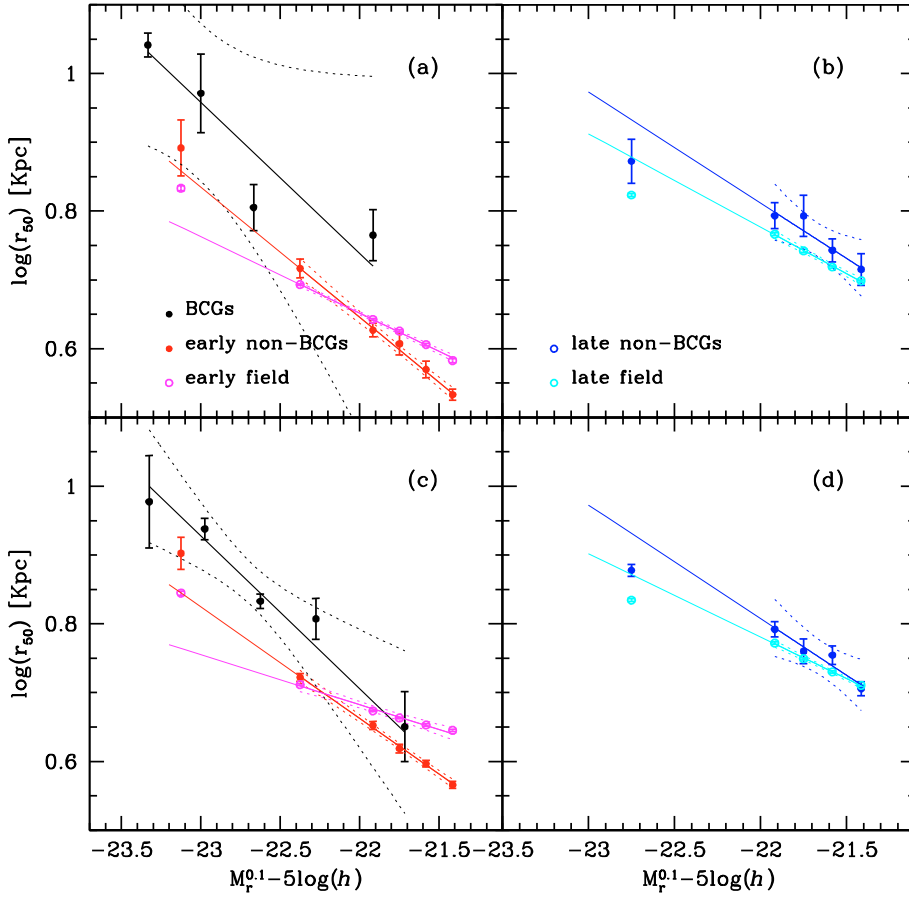


Fig. 6. The luminosity size relation: Median of $\log(r_{50})$ versus $M_r^{0.1}$ for the C-P04-I sample (*top panels*) and the C-K07-I sample (*bottom panels*). Error bars were obtained by the bootstrap re-sampling technique. Dotted lines show the 95% confidence bands of the linear regression. The red and magenta lines show the linear regression of non-BCGs early types in cluster and field respectively. The blue and cyan lines correspond to late types in cluster and field respectively. Black lines show the linear fits for BCGs.

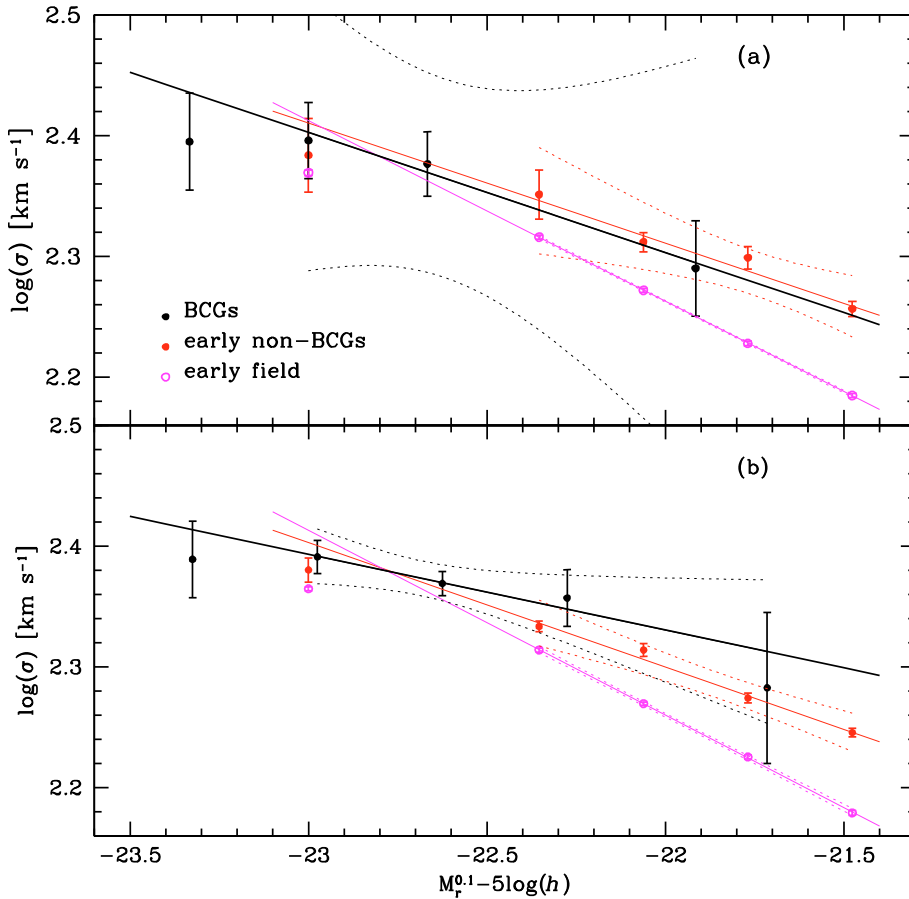


Fig. 7. Faber-Jackson Relation: Linear fits of $\log(\sigma)$ versus $M_r^{0.1}$ for non-BCGs early-types (red lines), BCGs (black lines) and control samples (magenta lines). The panels correspond to the same cases as in Fig. 6.

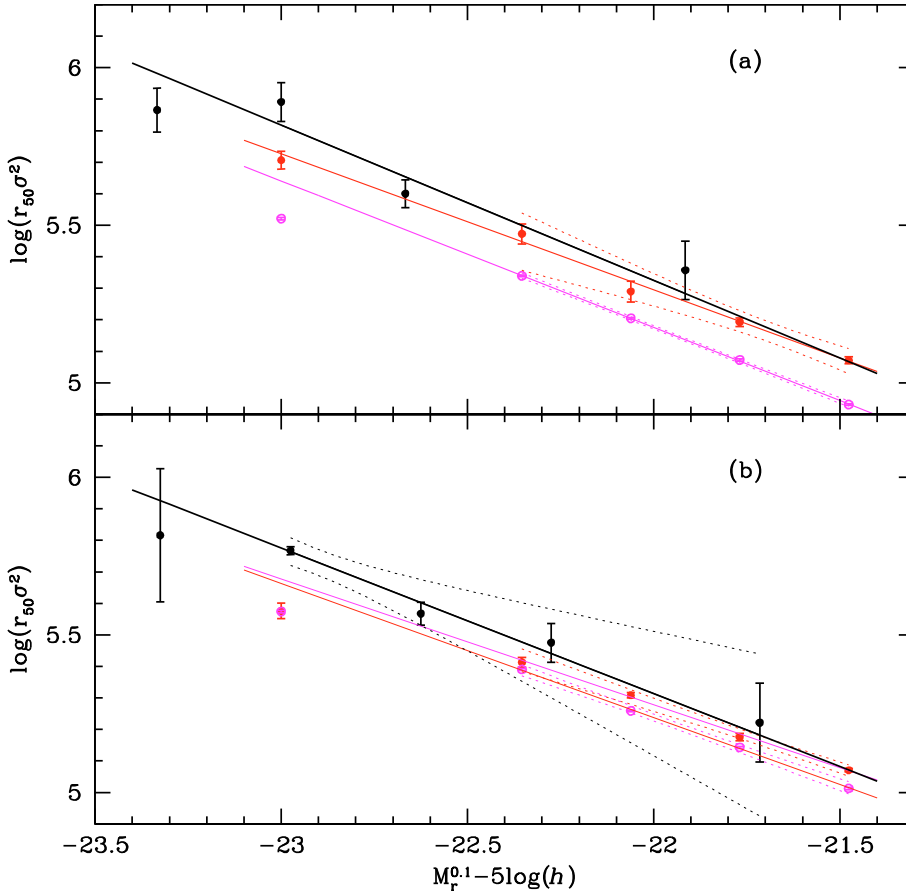


Fig. 8. Correlation between dynamical mass $r_{50\sigma^2}$ and luminosity for early-types (red lines), BCGs (black lines) and control samples (magenta lines), as in Fig. 7.

Table 3. Parameters of the fits $\log(\sigma) = -\frac{0.4}{\beta} M_r + b$, see Fig. 7.

	<i>early non-BCGs</i>	<i>BCGs</i>	<i>early field</i>
	C-P04-I		F-P04-E
β	4.0 ± 0.8	4 ± 2	2.67 ± 0.05
b	-0.1 ± 0.3	0 ± 1	-1.03 ± 0.06
	C-K07-I		F-K07-E
β	3.9 ± 0.2	7 ± 3	2.61 ± 0.05
b	0.0 ± 0.1	1.0 ± 0.7	-1.11 ± 0.06

Table 4. Parameters of the fits $\log(r_{50\sigma^2}) = aM_r + b$, see Fig. 8.

	<i>early non-BCGs</i>	<i>BCGs</i>	<i>early field</i>
	C-P04-I		F-P04-E
a	-0.43 ± 0.03	-0.5 ± 0.1	-0.464 ± 0.005
b	-4.2 ± 0.7	-6 ± 2	-5.0 ± 0.1
	C-K07-I		F-K07-E
a	-0.40 ± 0.01	-0.46 ± 0.05	-0.425 ± 0.005
b	-3.5 ± 0.3	-5 ± 1	-4.1 ± 0.1

4. Galaxy segregation

Using the C-P04-I and C-K07-I samples, Martínez et al. (2008) found that galaxy properties show a clear dependence on the clustocentric distance: a higher fraction of early type galaxies are found in the inner regions of clusters. In addition, they found that the $g-r$ colour is the property most predictive of the clustocentric distance of galaxies. Skibba et al. (2008) used SDSS galaxies with data from the Galaxy Zoo (Bamford et al. 2008) and found that for fixed morphology, the environmental dependence of colour remains strong. Blanton & Berlind (2007) found

that the relation between galaxy colors and the distance from the centre of groups has a residual relationship on the clustering of galaxies at small scales ($<300 h^{-1}$ Kpc). In this work we are interested in the study of the segregation of several properties of bright galaxies in clusters as a function of r/r_{200} and its dependence on the cluster identification techniques. Coenda et al. (2006) found that these type of analysis can produce different results depending on whether redshift-confirmed members or galaxies in projection are considered. Although we are only considering bright galaxies, our analysis is based on confirmed members in volume limited galaxy samples identified with two different criteria and galaxies extracted from the same galaxy catalogue. The characteristics of these samples make them suitable for an unbiased analysis of the properties of galaxies and its dependence on the cluster environment.

As we explained in Sect. 2.2, we have adopted several criteria to classify galaxies into morphological classes or types. We have used in our analysis the following parameters: the $g-r$ colour, the concentration index C , the *eclass* parameter and the Sersic index n . Although they are not independent, they are dominated by different physical properties of galaxies.

Figure 9 shows the fraction of early type galaxies as a function of the clustocentric radius. For both cluster samples a clear dependence of r/r_{200} with $g-r$, C and *eclass* is found (panels a) to c)). The correlation is up to $r/r_{200} \sim 1$, for larger clustocentric distances we do not see any tendency. For the Sersic index n (panel d)) we only observe a dependence for the C-K07-I sample. The comparison between the two cluster samples shows that the X-ray selected clusters always present a higher fraction of early type galaxies in the whole range of clustocentric distances. As it was pointed out previously, the X-ray sample has a slightly higher fraction of massive clusters than the MaxBCG

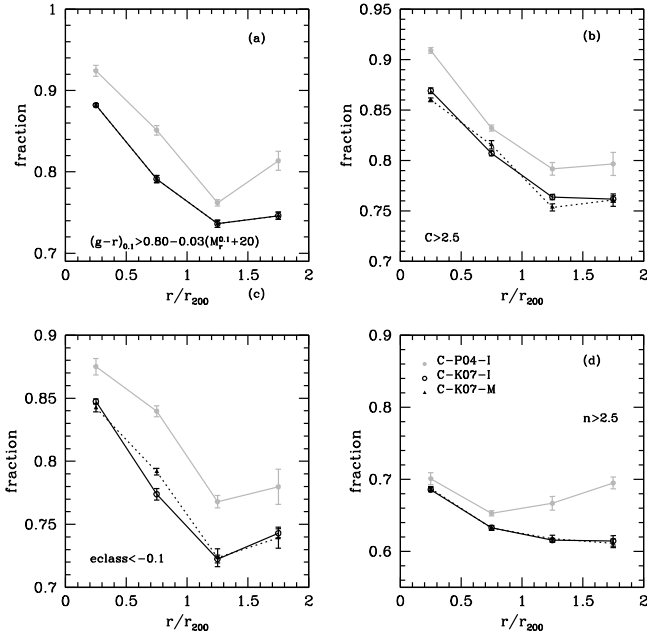


Fig. 9. Fraction of early type galaxies as a function of the normalized clustocentric radius. Early type galaxies are selected according to several parameters: $(g-r)^{0.1}$ in panel **a**), C in panel **b**), e_{class} in panel **c**) and n in panel **d**). The solid grey lines show the C-P04-I sample, whereas the solid black lines show the C-K07-I sample. The dotted black lines show the C-K07-M sample.

sample. In order to test if this difference in the mass distributions can be responsible for the higher fraction of early type galaxies in C-P04-I than in C-K07-I sample, we constructed a new subsample (C-K07-M) that consists of galaxies selected at random from C-K07-I having the same parent-cluster mass distribution as C-P04-I. As can be appreciated in Fig. 9, the fractions of early type galaxies as a function of r/r_{200} for C-K07-M (dotted lines) are indistinguishable from those corresponding to the C-K07-I sample, indicating that our finding of a higher fraction of early type galaxies in X-ray than in MaxBCG clusters is independent of the dynamical mass distribution.

In panel (a) of Fig. 10 we show the fraction of galaxies brighter than $M_r^{0.1} \leq -22.5$ as a function of the normalized clustocentric distance. Analogously to the morphological segregation, we can see a clear dependence of this fraction for $r/r_{200} \leq 1$, in the sense that galaxies brighter $M_r^{0.1} \leq -22.5$ preferentially inhabit the cluster centres. This trend is stronger for the C-K07-I sample. Alternatively, in panel (b) we show the median values of $M_r^{0.1}$ as a function r/r_{200} . We observe the dependence between the median $M_r^{0.1}$ and r/r_{200} for the C-K07-I sample. This effect is not observed for C-P04-I sample. The dispersion observed in mean values of $M_r^{0.1}$ (especially for C-P04-I sample) is due to the natural spread of the luminosity function.

As discussed in Sect. 3.1, the study of galaxy sizes and their relation to the luminosity helps to understand the galaxy formation and evolution. Here we study a possible dependence of galaxy size, r_{50} , as a function of r/r_{200} . Panel (a) in Fig. 11 shows the median value of r_{50} versus the normalized clustocentric distance, for the C-P04-I sample (grey line) and for the C-K07-I sample (black line). For clustocentric distances larger than 0.8, mean sizes of galaxies remain almost constant, being slightly larger for galaxies in X-ray clusters than in the MaxBCG sample, although the same effect is observed for field galaxies (horizontal dashed lines in Fig. 11). For smaller clustocentric distances, median sizes show different behaviour: for galaxies in the

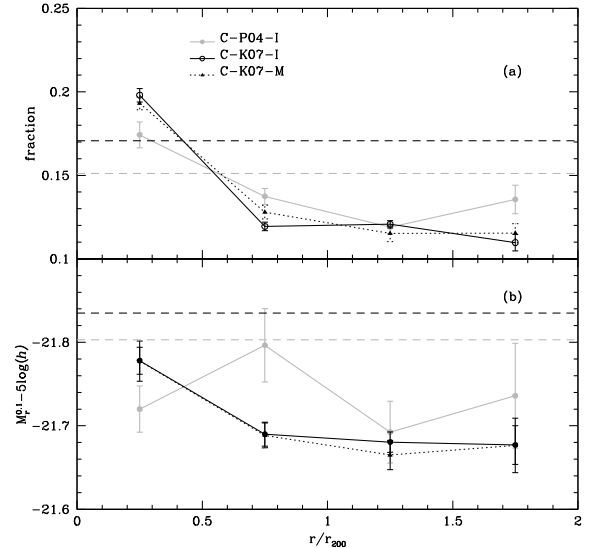


Fig. 10. Panel **a**) fraction of galaxies brighter than $M_r^{0.1} \leq -22.5$ as a function of r/r_{200} . The grey line shows the C-P04-I sample while the black line corresponds to the C-K07-I sample. The horizontal dashed lines show the median values of the corresponding field samples in the same colors as their cluster counterparts. Panel **b**) median values of $M_r^{0.1}$ versus r/r_{200} . The horizontal lines show the median values of the corresponding field samples.

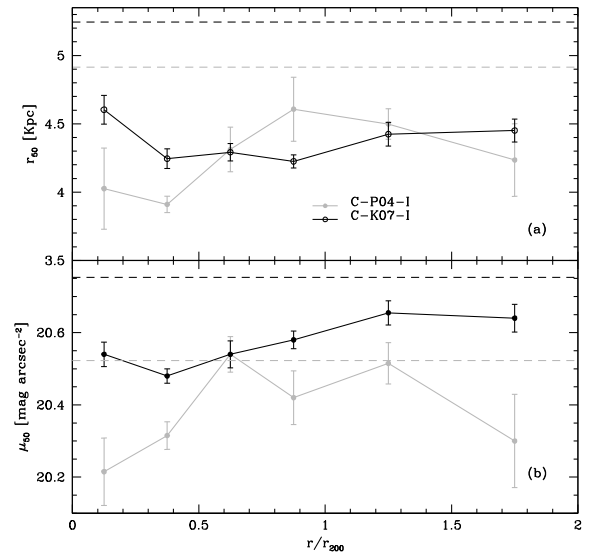


Fig. 11. Panel **a**) shows the median values of r_{50} versus r/r_{200} and panel **b**) the median values of μ_{50} versus r/r_{200} . The horizontal lines show the median values of the corresponding field samples, as in Fig. 10.

C-P04-I sample, median values of r_{50} decrease as r/r_{200} goes to zero, whereas the opposite behaviour is observed for galaxies in the C-K07-I sample. Panel (b) in Fig. 11 shows the median value of the r -band surface brightness μ_{50} , computed inside r_{50} , as a function of r/r_{200} . For both cluster samples, μ_{50} decreases as r/r_{200} goes to zero. Field galaxies have lower surface brightness (black horizontal line) than cluster members.

Figure 12 repeats the previous analysis using only early type galaxies. In the left panels we show this relation for the C-P04-I sample while C-K07-I sample are shown in the right panels. We have also evaluated the influence of BCG_s in our results, repeating the analysis without BCG_s (dotted lines). Analogously to Fig. 11, the sizes of early type galaxies increase when r/r_{200} decreases in the C-K07-I sample. Nevertheless, this tendency

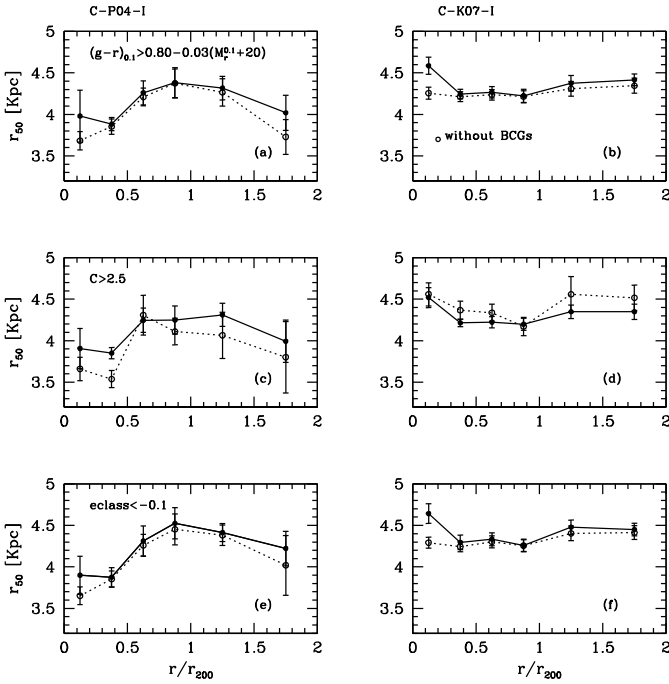


Fig. 12. Median values of r_{50} as a function of r/r_{200} for early-type galaxies. In the *left panels* we show this relation for the C-P04-I sample while C-K07-I clusters are shown on the *right panels*. Early type galaxies were selected according to several parameters: $(g-r)^{0.1}$ in **a)** and **b)**, C in **c)** and **d)**, and e_{class} in **e)** and **f)**. Dotted lines show the same relation but excluding the BCG_s .

disappears when BCG_s are excluded. On the other hand, the median values of r_{50} decrease as r/r_{200} goes to zero for the C-P04-I sample; this effect is stronger when BCG_s are excluded. These results clearly show an important difference between clusters identified with different criteria. As can be appreciated in Fig. 3, a higher fraction of early type galaxies is observed for the X-ray selected clusters. Consequently, the different behaviour observed in Fig. 12, could be the result of the differences in the population of early type galaxies between the two samples. For instance, a higher fraction of elliptical galaxies in the early type population of the X-ray selected clusters with respect to the MaxBCG sample could produce a different behaviour in the mean sizes as a function of r/r_{200} . In order to test this possibility, we repeated the analysis of Fig. 12 selecting early type galaxies with $C > 3.1$. This new threshold includes a third of the early type galaxies previously analyzed, and it will mostly select elliptical galaxies. For this sub-sample of early type galaxies, we find the same trend observed in Fig. 12, confirming that there is a dependence of the mean sizes of early type galaxies on the cluster selection criterion. Based on a sample of 228 elliptical galaxies in 24 clusters, Cypriano et al. (2006) found that elliptical galaxies in the inner regions of clusters are typically 5% smaller than those in the outer regions. These authors interpreted these results in terms of the tidal stripping of stars that lead to changes in the whole structure of galaxies in the central regions of clusters.

Figure 13 is the analogous of Fig. 12 for late-type galaxies. Although galaxies in X-ray selected clusters show a tendency on average r_{50} to be smaller towards the cluster centers, this behaviour is not statistically significant.

5. Discussion and conclusions

We have compiled two catalogues of massive clusters of galaxies based on samples that make use of different identification

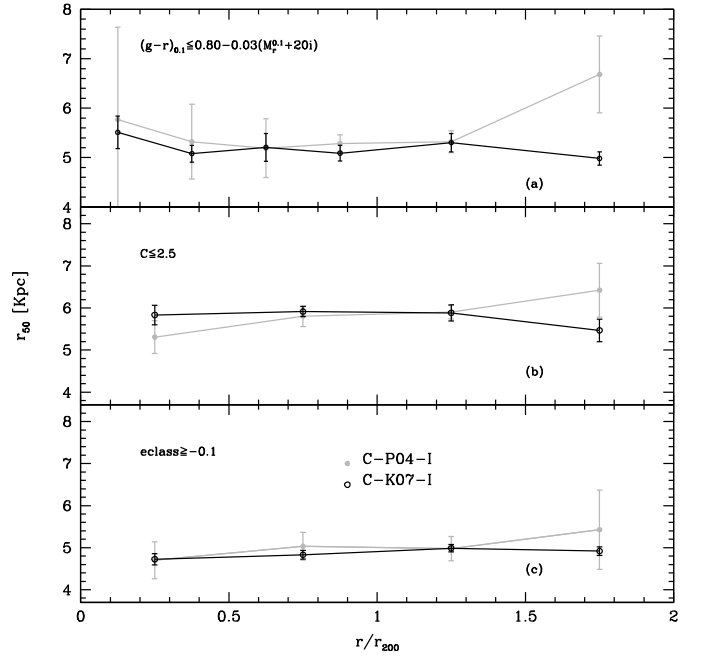


Fig. 13. Median values of r_{50} as a function of r/r_{200} for late-type galaxies, analogously to Fig. 12.

techniques: the P04 sample that comprises bright X-ray galaxy clusters and the K07 sample, constructed according to the properties of early-type galaxies. We selected sub-samples of galaxy clusters in the redshift range $0.05 < z < 0.14$. For both samples, member galaxies are brighter than $M_r^{0.1} = -21.3$ and were identified from a spectroscopic volume-limited sample of the DR5-SDSS. In order to select a fair sample of clusters of galaxies we use the *fof* algorithm and an eyeball examination of each overdensity identified by *fof*. Throughout the visual inspection, we classified the clusters based on their substructure. We only consider in our analysis regular clusters and we exclude systems that have two or more close substructures of similar size in the plane of the sky and/or in the redshift distribution. In addition, we have determined new positions in the plane of the sky and in the line of sight. We found that for $\sim 40\%$ of the clusters, the angular position given by *fof* is better than the original value, whereas for $\sim 17\%$ of the clusters, the redshift given by *fof* is a better match to the observed mean redshift distribution than the original value. Our final sample comprises 49 X-ray selected clusters with 786 galaxies and 209 MaxBCG clusters with 3041 galaxies. We have determined the following physical properties of clusters: the line-of-sight velocity dispersion σ , the virial radius and mass and r_{200} .

We have analyzed different scaling relations between photometric and dynamical parameters. Bright galaxies were separated in early and late types according to several criteria. We have also studied the segregation of galaxies analysing different properties as a function of the normalized clustocentric distances. The main results are:

- Galaxies in X-ray and MaxBCG selected clusters show similar size-luminosity relations.
- We found that each galaxy type has a different luminosity-size relation. This implies a different mass-luminosity relation and/or a different star formation history.
- For each luminosity bin, late type galaxies in the field have sizes smaller than their cluster counterpart.

- The same effect is observed for early type galaxies, although the differences are smaller. The stronger effect corresponds to galaxies in MaxBCG clusters.
- At fixed luminosity, BCG_s tend to be larger and show a steeper $\log(r_{50}) - M_r^{0.1}$ relation than non-BCG early type galaxies in clusters.
- Non-BCGs early type galaxies in clusters and in the field show the known curvature in the size-luminosity relation.
- The Faber-Jackson relation for early-type galaxies in clusters is the same in X-ray and MaxBCG clusters.
- We found a clear difference between galaxies in clusters (both BCG_s and non-BCG) and in the field, showing the later lower values of the velocity dispersion at fixed luminosity.
- The $\log \sigma - M_r^{0.1}$ relation presents, at the bright end, a departure from linearity. Bright early type galaxies show a lower velocity dispersion than the expected from the linear relation at lower magnitudes.
- BCG_s show a flatter $\log \sigma - M_r^{0.1}$ relation than non-BCG galaxies. Nevertheless, the velocity dispersion of the brightest non-BCG galaxies are consistent with the values expected for BCG_s .
- At fixed luminosity, BCG_s have, on average, higher dynamical masses than early-type galaxies in clusters. The difference is more significant for MaxBCG clusters than for X-ray selected clusters.
- At fixed luminosity, field early type galaxies in the control samples show lower dynamical masses than non-BCG early type galaxies in clusters.
- Using several criteria to classify galaxies into morphological classes, we found the well know morphological segregation for both samples of clusters. The correlation is up to $r/r_{200} \sim 1$; for larger clustocentric distances we do not see any trend.
- For the whole range of clustocentric distances, X-ray selected clusters have a higher fraction of early type galaxies than MaxBCG clusters.
- Within $r/r_{200} \sim 1$ we found a dependence of the fraction of galaxies brighter than $M_r^{0.1} \leq -22.5$ as a function of the normalized clustocentric distance. Bright galaxies preferentially inhabit the cluster centers. This tendency is stronger for MaxBCG clusters.
- For clustocentric distances larger than 0.8, mean sizes of galaxies remain almost constant, being slightly larger for galaxies in X-ray selected clusters than in the MaxBCG sample.
- For $r/r_{200} \leq 0.8$, median sizes depend on the cluster sample. For galaxies in X-ray selected clusters, median values of r_{50} decrease as r/r_{200} goes to zero, whereas the opposite is observed for galaxies in the MaxBCG clusters.
- For MaxBCG clusters, the sizes of early type galaxies increase as r/r_{200} decreases. The trend disappears when BCG_s are excluded. On the contrary, the median value of r_{50} decrease as r/r_{200} goes to zero for X-ray selected clusters. The effect is stronger when BCG_s are excluded.

Early type galaxies in the field are lower, have lower velocity dispersion and have smaller virial masses than their cluster counterpart. On the other hand, BCG_s are larger and have higher values of the virial masses than non-BCG in clusters, although the velocity dispersions are comparable. These differences in the properties of early type galaxies in the field, in clusters and with BCG_s are consistent with the scenario where the environment plays a fundamental rol in the formation histories of galaxies. These results suggest three different formation scenarios, BCG_s being the galaxies less affected by dissipation. Dry mergers have

no energy loss mechanism, therefore the formed galaxies are less centrally contracted with optical sizes larger than those of galaxies that have undergone a dissipative merger (Kormendy 1989; Nipoti et al. 2003; Bernardi et al. 2007). Weinmann et al. (2009) and Guo et al. (2009) analyzed the size-luminosity relation of galaxies in groups, where the environmental effects are supposed to be different to those expected in clusters. These authors found the same size-luminosity relation for both central and satellite early type galaxies. The different results between galaxies in groups and clusters also support the idea that the size-luminosity relation depends on the environment.

At the same luminosity, late-type galaxies in clusters have larger sizes, and therefore lower surface brightness than their field counterparts (control sample). This is in agreement with the scenario of strangulation (Larson et al. 1980), where the gas in the halo is stripped, suppressing the supply of cold gas and therefore affecting the star formation rate and the galaxy luminosity.

The X-ray selected sample C-P04-I is made of bright X-ray galaxy clusters, whereas the C-K07-I sample was constructed according to the properties of early-type galaxies. Several clusters in the C-K07-I sample should be X-ray emitters, although they would be, on average, less X-ray luminous than C-P04-I clusters. The fact that X-ray selected clusters show a higher fraction of early type galaxies whose sizes tend to decrease towards the cluster center, effect that is not observed for galaxies in MaxBCG clusters, can be interpreted as possible evidence that the hot intracluster medium is also playing a role in the evolution of early type galaxies. Alternatively, the observed effect could be caused by differences in the clusters masses. Even though the effects mentioned above are also present for sub-samples of C-P04-I and C-K07-I with the same virial mass distribution, due to the usual uncertainties in the computation of these masses, we cannot discard differences in the actual mass distributions. If this is the case, and C-P04-I clusters are on average more massive than C-K07-I, decreases in the mean sizes of early type galaxies in X-ray selected clusters could be the result of tidal stripping that can produce changes in the structure of galaxies (see the results from numerical simulations of Aguilar & White (1986) and observational evidences from Trujillo et al. (2002) and Cypriano et al. (2006)). This difference between X-ray and MaxBCG selected clusters is an unexpected result that should be explored in more detail.

Acknowledgements. This work has been partially supported with grants from Consejo Nacional de Investigaciones Científicas y Técnicas de la República Argentina (CONICET) and Secretaría de Ciencia y Tecnología de la Universidad de Córdoba. We kindly thank Dr. Héctor J. Martínez for his helpful comments on the manuscript, which contributed to improve the present paper. VC acknowledges the guidance of Dr. Ariel Zandivarez in the construction of the cluster sample.

References

- Adelman-McCarthy, J. K., Agüeros, M. A., Allam, S. S., et al. 2007, ApJS, 172, 634
- Adelman-McCarthy, J. K., Agüeros, M. A., Allam, S. S., et al. 2008, ApJS, 175, 297
- Aguilar, L. A., & White, S. D. M. 1986, ApJ, 307, 97
- Andredakis, Y. C., Peletier, R. F., & Balcells, M. 1995, MNRAS, 275, 874
- Bahcall, N. A. 1973, ApJ, 183, 783
- Ball, N. M., Loveday, J., & Brunner, R. J. 2008, MNRAS, 383, 907
- Bamford, S. P., Rojas, A. L., Nichol, R. C., et al. 2008, MNRAS, 391, 607
- Beers, T. C., Flynn, K., & Gebhardt, K. 1990, AJ, 100, 32
- Bernardi, M. 2009, MNRAS, 510
- Bernardi, M., Sheth, R. K., Annis, J., et al. 2003, AJ, 125, 1866
- Bernardi, M., Sheth, R. K., Nichol, R. C., Schneider, D. P., & Brinkmann, J. 2005, AJ, 129, 61

- Bernardi, M., Hyde, J. B., Sheth, R. K., Miller, C. J., & Nichol, R. C. 2007, *AJ*, 133, 1741
- Bildfell, C., Hoekstra, H., Babul, A., & Mahdavi, A. 2008, *MNRAS*, 384, 934
- Biviano, A., Katgert, P., Thomas, T., & Adami, C. 2002, *A&A*, 387, 8
- Blanton, M. R., & Berlind, A. A. 2007, *ApJ*, 664, 791
- Blanton, M. R., Brinkmann, J., Csabai, I., et al. 2003, *AJ*, 125, 2348
- Blanton, M. R., Eisenstein, D., Hogg, D. W., Schlegel, D. J., & Brinkmann, J. 2005a, *ApJ*, 629, 143
- Blanton, M. R., Schlegel, D. J., Strauss, M. A., et al. 2005b, *AJ*, 129, 2562
- Carlberg, R. G., Yee, H. K. C., & Ellingson, E. 1997, *ApJ*, 478, 462
- Coenda, V., Donzelli, C. J., Muriel, H., et al. 2005, *AJ*, 129, 1237
- Coenda, V., Muriel, H., Donzelli, C. J., et al. 2006, *AJ*, 131, 1989
- Cross, N. J. G., Bouwens, R. J., Benítez, N., et al. 2004, *AJ*, 128, 1990
- Cypriano, E. S., Sodré, L. J., Campusano, L. E., Dale, D. A., & Hardy, E. 2006, *AJ*, 131, 2417
- de Jong, R. S., & Lacey, C. 2000, *ApJ*, 545, 781
- Díaz, E., Zandivarez, A., Merchán, M. E., & Muriel, H. 2005, *ApJ*, 629, 158
- Djorgovski, S., & Davis, M. 1987, *ApJ*, 313, 59
- Domínguez, M., Muriel, H., & Lambas, D. G. 2001, *AJ*, 121, 1266
- Dressler, A. 1980, *ApJS*, 42, 565
- Dressler, A., Lynden-Bell, D., Burstein, D., et al. 1987, *ApJ*, 313, 42
- Dressler, A., Oemler, A. J., Couch, W. J., et al. 1997, *ApJ*, 490, 577
- Driver, S. P., Odewahn, S. C., Echevarria, L., et al. 2003, *AJ*, 126, 2662
- Driver, S. P., Allen, P. D., Graham, A. W., et al. 2006, *MNRAS*, 368, 414
- Faber, S. M., & Jackson, R. E. 1976, *ApJ*, 204, 668
- Ferguson, H. C., Dickinson, M., Giavalisco, M., et al. 2004, *ApJ*, 600, L107
- Folkes, S., Ronen, S., Price, I., et al. 1999, *MNRAS*, 308, 459
- Girardi, M., Biviano, A., Giuricin, G., Mardirossian, F., & Mezzetti, M. 1993, *ApJ*, 404, 38
- Goto, T., Sekiguchi, M., Nichol, R. C., et al. 2002, *AJ*, 123, 1807
- Guo, Y., McIntosh, D. H., Mo, H. J., et al. 2009, *ArXiv e-prints*
- Huchra, J. P., & Geller, M. J. 1982, *ApJ*, 257, 423
- Hyde, J. B., & Bernardi, M. 2009, *MNRAS*, 349, 1
- Kashikawa, N., Sekiguchi, M., Doi, M., et al. 1998, *ApJ*, 500, 750
- Koester, B. P., McKay, T. A., Annis, J., et al. 2007a, *ApJ*, 660, 239
- Koester, B. P., McKay, T. A., Annis, J., et al. 2007b, *ApJ*, 660, 221
- Kormendy, J. 1977, *ApJ*, 218, 333
- Kormendy, J. 1989, *ApJ*, 342, L63
- La Barbera, F., Merluzzi, P., Busarello, G., Massarotti, M., & Mercurio, A. 2004, *A&A*, 425, 797
- Larson, R. B., Tinsley, B. M., & Caldwell, C. N. 1980, *ApJ*, 237, 692
- Lauer, T. R., Faber, S. M., Richstone, D., et al. 2007, *ApJ*, 662, 808
- Liu, F. S., Xia, X. Y., Mao, S., Wu, H., & Deng, Z. G. 2007, *ArXiv e-prints*, 712
- Lobo, C., Biviano, A., Durret, F., et al. 1997, *A&A*, 317, 385
- Loveday, J., Peterson, B. A., Efstathiou, G., & Maddox, S. J. 1992, *ApJ*, 390, 338
- Madgwick, D. S., Lahav, O., Baldry, I. K., et al. 2002, *MNRAS*, 333, 133
- Malumuth, E. M., & Kirshner, R. P. 1981, *ApJ*, 251, 508
- Malumuth, E. M., & Kirshner, R. P. 1985, *ApJ*, 291, 8
- Martínez, H. J., Coenda, V., & Muriel, H. 2008, [[arXiv:0809.1585](https://arxiv.org/abs/0809.1585)]
- McIntosh, D. H., Bell, E. F., Rix, H.-W., et al. 2005, *ApJ*, 632, 191
- Melnick, J., & Sargent, W. L. W. 1977, *ApJ*, 215, 401
- Merchán, M. E., & Zandivarez, A. 2005, *ApJ*, 630, 759
- Miller, C. J., Nichol, R. C., Reichart, D., et al. 2005, *AJ*, 130, 968
- Möllenhoff, C., & Heidt, J. 2001, *A&A*, 368, 16
- Nipoti, C., Londrillo, P., & Ciotti, L. 2003, *MNRAS*, 342, 501
- Noonan, T. 1961, *PASP*, 73, 212
- Oegerle, W. R., & Hoessel, J. G. 1991, *ApJ*, 375, 15
- Oemler, A. J. 1974, *ApJ*, 194, 1
- Peng, C. Y., Ho, L. C., Impey, C. D., & Rix, H.-W. 2002, *AJ*, 124, 266
- Petrosian, V. 1976, *ApJ*, 209, L1
- Popesso, P., Böhringer, H., Brinkmann, J., Voges, W., & York, D. G. 2004, *A&A*, 423, 449
- Pracy, M. B., Driver, S. P., De Propris, R., Couch, W. J., & Nulsen, P. E. J. 2005, *MNRAS*, 364, 1147
- Rood, H. J., & Turnrose, B. E. 1968, *ApJ*, 152, 1057
- Sandage, A., & Perelmuter, J.-M. 1990, *ApJ*, 361, 1
- Sandage, A., & Visvanathan, N. 1978a, *ApJ*, 225, 742
- Sandage, A., & Visvanathan, N. 1978b, *ApJ*, 223, 707
- Schechter, P. 1976, *ApJ*, 203, 297
- Schlegel, D. J., Finkbeiner, D. P., & Davis, M. 1998, *ApJ*, 500, 525
- Sérsic, J. L. 1963, *Boletín de la Asociación Argentina de Astronomía*, 6, 41
- Sérsic, J. L. 1968, *Atlas de galaxias australes (Córdoba, Argentina: Observatorio Astronómico)*
- Shen, S., Mo, H. J., White, S. D. M., et al. 2003, *MNRAS*, 343, 978
- Shimasaku, K., Fukugita, M., Doi, M., et al. 2001, *AJ*, 122, 1238
- Skibba, R. A., Bamford, S. P., Nichol, R. C., et al. 2008, *ArXiv e-prints*
- Strateva, I., Ivezić, Ž., Knapp, G. R., et al. 2001, *AJ*, 122, 1861
- Strauss, M. A., Weinberg, D. H., Lupton, R. H., et al. 2002, *AJ*, 124, 1810
- Syer, D., Mao, S., & Mo, H. J. 1999, *MNRAS*, 305, 357
- Trujillo, I., Aguerrí, J. A. L., Gutiérrez, C. M., Caon, N., & Cepa, J. 2002, *ApJ*, 573, L9
- Trujillo, I., Förster Schreiber, N. M., Rudnick, G., et al. 2006, *ApJ*, 650, 18
- Tully, R. B., & Fisher, J. R. 1977, *A&A*, 54, 661
- von der Linden, A., Best, P. N., Kauffmann, G., & White, S. D. M. 2007, *MNRAS*, 379, 867
- Weinmann, S. M., Kauffmann, G., van den Bosch, F. C., et al. 2009, *MNRAS*, 394, 1213
- Whitmore, B. C., Gilmore, D. M., & Jones, C. 1993, *ApJ*, 407, 489
- Yang, X., Mo, H. J., van den Bosch, F. C., et al. 2007, *ApJ*, 671, 153
- Yepes, G., Domínguez-Tenreiro, R., & del Pozo-Sanz, R. 1991, *ApJ*, 373, 336
- Yip, C. W., Connolly, A. J., Szalay, A. S., et al. 2004, *AJ*, 128, 585
- York, D. G., Anderson, Jr., J. E., Anderson, S. F., et al. 2000, *AJ*, 120, 1579
- Ziegler, B. L., Saglia, R. P., Bender, R., et al. 1999, *A&A*, 346, 13

Table A.1. C-P04-I cluster sample.

α (J2000.00)	δ (J2000.00)	z	σ	M_{vir}	R_{vir}	R_{200}
[h m s]	[$^{\circ}$ ' "]		[km s $^{-1}$]	[$h^{-1} M_{\odot}$]	[h^{-1} Mpc]	[h^{-1} Mpc]
0 41 50.1	-9 18 6.8	0.056	698.82	0.558×10^{15}	1.638	1.729
1 19 37.7	+14 53 35.2	0.129	778.90	0.502×10^{15}	1.185	1.927
7 36 25.0	+39 25 58.4	0.117	605.19	0.482×10^{15}	1.887	1.497
7 53 19.0	+29 22 26.8	0.061	689.22	0.606×10^{15}	1.829	1.705
8 9 40.2	+34 55 34.3	0.082	528.46	0.323×10^{15}	1.656	1.308
8 10 22.6	+42 16 0.8	0.064	548.75	0.292×10^{15}	1.391	1.358
8 22 10.0	+47 5 58.2	0.130	674.55	0.671×10^{15}	2.114	1.669
8 25 27.6	+47 7 10.6	0.126	792.06	0.952×10^{15}	2.175	1.960
8 28 6.7	+44 45 48.2	0.145	577.57	0.187×10^{15}	0.803	1.429
8 45 29.0	+44 34 28.2	0.054	331.69	0.545×10^{14}	0.710	0.821
9 13 9.2	+47 43 26.4	0.052	408.98	0.120×10^{15}	1.032	1.012
9 53 41.5	+1 42 42.5	0.098	403.63	0.165×10^{15}	1.454	0.999
10 23 41.1	+49 8 5.6	0.144	618.10	0.532×10^{15}	1.997	1.529
10 54 5.5	+54 50 50.6	0.072	448.67	0.192×10^{15}	1.368	1.110
10 58 26.3	+56 47 31.9	0.136	597.87	0.332×10^{15}	1.330	1.479
11 13 22.7	+2 32 32.6	0.075	431.97	0.170×10^{15}	1.304	1.069
11 15 32.2	+54 26 5.6	0.070	628.67	0.334×10^{15}	1.213	1.556
11 21 36.2	+48 3 50.0	0.112	728.02	0.541×10^{15}	1.462	1.801
11 33 17.3	+66 22 45.5	0.115	847.57	0.934×10^{15}	1.865	2.097
11 44 8.2	+5 45 22.7	0.103	586.83	0.370×10^{15}	1.541	1.452
11 44 40.8	+67 24 40.0	0.117	453.55	0.221×10^{15}	1.542	1.122
12 0 24.5	+3 19 51.6	0.133	858.09	0.119×10^{16}	2.310	2.123
12 17 40.8	+3 39 41.0	0.077	922.14	0.113×10^{16}	1.903	2.282
12 58 41.1	-1 45 24.8	0.084	740.78	0.769×10^{15}	2.010	1.833
13 2 50.7	-2 30 22.3	0.083	681.06	0.534×10^{15}	1.650	1.685
13 3 56.5	+67 31 3.7	0.106	659.69	0.358×10^{15}	1.179	1.632
13 9 17.0	-1 36 45.4	0.083	519.51	0.238×10^{15}	1.264	1.285
13 26 17.8	+0 13 32.5	0.082	501.04	0.242×10^{15}	1.382	1.240
13 30 49.9	-1 52 22.1	0.087	659.17	0.480×10^{15}	1.585	1.631
13 32 38.9	+54 19 9.5	0.101	811.68	0.927×10^{15}	2.018	2.008
13 36 6.5	+59 12 26.6	0.071	934.40	0.123×10^{16}	2.017	2.312
13 42 28.3	+2 14 45.2	0.077	752.26	0.686×10^{15}	1.738	1.861
13 53 0.8	+5 9 21.2	0.079	755.36	0.579×10^{15}	1.454	1.869
14 14 47.4	-0 23 56.8	0.140	612.45	0.448×10^{15}	1.712	1.515
14 24 40.4	+2 44 46.7	0.055	558.59	0.208×10^{15}	0.954	1.382
14 25 22.9	+63 11 22.6	0.139	1052.31	0.198×10^{16}	2.557	2.604
15 12 51.1	-1 28 47.3	0.122	812.48	0.895×10^{15}	1.943	2.010
15 16 34.0	-0 56 55.7	0.118	539.58	0.385×10^{15}	1.897	1.335
15 29 12.1	+52 50 39.8	0.074	694.40	0.522×10^{15}	1.553	1.718
16 1 22.1	+53 54 19.1	0.106	491.24	0.284×10^{15}	1.686	1.216
16 11 17.7	+36 57 38.2	0.067	529.83	0.275×10^{15}	1.406	1.311
16 56 20.3	+39 16 59.9	0.062	440.23	0.140×10^{15}	1.034	1.089
16 59 45.4	+32 36 58.0	0.101	512.65	0.257×10^{15}	1.403	1.268
17 2 42.6	+34 3 40.7	0.099	1060.16	0.161×10^{16}	2.059	2.623
17 12 47.6	+64 3 47.5	0.080	1037.59	0.167×10^{16}	2.223	2.567
17 18 9.9	+56 39 59.0	0.113	676.01	0.565×10^{15}	1.772	1.673
21 24 56.3	-6 56 47.4	0.118	809.90	0.102×10^{16}	2.224	2.004
21 57 25.8	-7 47 40.6	0.058	649.63	0.498×10^{15}	1.692	1.607
22 16 15.5	-9 20 23.6	0.084	488.35	0.218×10^{15}	1.311	1.208

Table A.2. Analogous to Table A.1, for C-K07-I cluster sample.

α (J2000.00)	δ (J2000.00)	z	σ	M_{vir}	R_{vir}	R_{200}
[h m s]	[° ' '']		[km s ⁻¹]	[$h^{-1} M_{\odot}$]	[h^{-1} Mpc]	[h^{-1} Mpc]
15 58 18.4	+27 16 12.0	0.090	1070.73	0.221×10^{16}	2.766	2.649
15 10 1.7	+33 28 24.2	0.110	844.46	0.841×10^{15}	1.691	2.089
13 25 16.7	+57 37 1.2	0.116	747.53	0.772×10^{15}	1.980	1.850
10 19 55.6	+40 59 23.3	0.092	899.02	0.747×10^{15}	1.325	2.224
16 42 38.6	+27 26 24.0	0.104	983.57	0.145×10^{16}	2.151	2.434
14 28 30.8	+56 48 18.7	0.106	776.22	0.875×10^{15}	2.081	1.921
10 27 46.8	+10 32 26.9	0.109	673.64	0.438×10^{15}	1.383	1.667
15 39 50.6	+30 42 36.0	0.097	751.73	0.647×10^{15}	1.642	1.860
14 35 20.0	+55 10 58.1	0.140	910.40	0.121×10^{16}	2.095	2.253
8 54 15.1	+29 3 30.6	0.085	670.67	0.409×10^{15}	1.305	1.659
14 58 44.4	+47 32 24.0	0.085	603.92	0.450×10^{15}	1.767	1.494
8 18 9.8	+54 35 39.1	0.118	438.81	0.216×10^{15}	1.607	1.086
12 33 13.9	+67 7 12.0	0.105	1000.66	0.202×10^{16}	2.888	2.476
9 1 30.1	+55 39 16.6	0.116	979.65	0.547×10^{15}	0.817	2.424
8 54 51.5	+0 50 50.3	0.108	685.18	0.525×10^{15}	1.604	1.695
15 24 11.8	+29 51 22.0	0.114	1219.20	0.215×10^{16}	2.072	3.017
15 24 32.0	+29 43 38.6	0.112	1100.42	0.203×10^{16}	2.404	2.723
15 47 41.5	+33 19 53.0	0.114	518.23	0.285×10^{15}	1.519	1.282
9 23 26.9	+8 39 2.5	0.129	844.89	0.996×10^{15}	2.001	2.091
11 53 51.2	+15 26 35.9	0.113	748.88	0.551×10^{15}	1.409	1.853
16 20 31.1	+29 53 27.6	0.097	853.98	0.103×10^{16}	2.030	2.113
16 3 19.8	+25 27 13.3	0.088	582.84	0.271×10^{15}	1.143	1.442
14 54 37.1	+54 25 23.2	0.100	630.37	0.423×10^{15}	1.525	1.560
21 30 27.0	-0 0 24.5	0.135	555.00	0.317×10^{15}	1.478	1.373
15 19 33.7	+4 20 16.8	0.103	664.20	0.361×10^{15}	1.173	1.643
21 49 4.6	-8 10 49.4	0.133	880.13	0.857×10^{15}	1.586	2.178
8 50 7.1	+29 32 52.1	0.104	730.39	0.707×10^{15}	1.899	1.807
8 54 57.5	+35 24 51.8	0.146	1271.75	0.245×10^{16}	2.170	3.147
14 29 21.1	+23 6 29.9	0.138	716.15	0.493×10^{15}	1.379	1.772
11 40 33.9	+10 21 41.0	0.105	412.45	0.143×10^{15}	1.201	1.021
11 13 48.5	-0 24 30.6	0.100	561.71	0.369×10^{15}	1.677	1.390
16 47 40.6	+29 55 18.1	0.099	1004.14	0.103×10^{16}	1.470	2.485
9 7 56.8	+52 48 2.9	0.099	732.91	0.462×10^{15}	1.232	1.813
10 9 34.3	+44 42 38.5	0.146	1080.56	0.161×10^{16}	1.974	2.674
10 8 0.4	+38 1 5.9	0.112	574.80	0.397×10^{15}	1.725	1.422
10 35 48.9	+36 5 58.6	0.123	462.89	0.169×10^{15}	1.134	1.145
14 7 46.5	+14 0 11.9	0.135	658.33	0.458×10^{15}	1.515	1.629
11 20 24.7	+47 9 26.3	0.112	605.14	0.425×10^{15}	1.664	1.497
10 41 34.6	-0 36 53.6	0.135	793.10	0.753×10^{15}	1.717	1.962
2 25 19.2	-8 44 5.3	0.054	479.32	0.131×10^{15}	0.817	1.186
0 28 22.5	+13 52 23.5	0.141	578.78	0.496×10^{15}	2.125	1.432
12 12 52.5	+6 3 48.2	0.137	580.40	0.353×10^{15}	1.502	1.436
12 47 20.0	+0 8 39.1	0.089	779.99	0.680×10^{15}	1.604	1.930
14 47 33.3	+33 2 38.4	0.087	314.85	0.901×10^{14}	1.303	0.779
15 29 1.3	+30 46 20.6	0.105	647.03	0.413×10^{15}	1.414	1.601
8 29 29.4	+39 9 27.7	0.092	659.36	0.417×10^{15}	1.376	1.632
1 1 3.3	-9 57 34.6	0.150	776.20	0.765×10^{15}	1.820	1.921
13 21 54.0	+57 32 21.5	0.118	379.97	0.121×10^{15}	1.201	0.940
20 51 42.2	-0 4 8.0	0.108	468.59	0.180×10^{15}	1.177	1.159
21 26 36.9	-6 39 13.0	0.124	513.26	0.291×10^{15}	1.584	1.270
12 4 8.3	+4 19 33.2	0.136	737.57	0.654×10^{15}	1.724	1.825
15 16 46.1	-0 54 2.9	0.118	877.76	0.118×10^{16}	2.204	2.172
10 58 1.5	+41 2 47.8	0.129	919.45	0.867×10^{15}	1.471	2.275
11 21 26.4	+53 44 56.8	0.104	694.49	0.536×10^{15}	1.592	1.718
8 14 52.7	+6 57 42.8	0.110	575.06	0.283×10^{15}	1.225	1.423
12 48 40.0	+62 37 3.0	0.104	640.81	0.294×10^{15}	1.025	1.586
16 45 37.9	+27 18 45.0	0.101	511.66	0.188×10^{15}	1.029	1.266
9 15 57.8	+5 29 0.6	0.142	624.91	0.445×10^{15}	1.633	1.546

Table A.2. continued.

α (J2000.00)	δ (J2000.00)	z	σ	M_{vir}	R_{vir}	R_{200}
[h m s]	[$^{\circ}$ ' "]		[km s $^{-1}$]	[$h^{-1} M_{\odot}$]	[h^{-1} Mpc]	[h^{-1} Mpc]
10 20 15.3	+39 18 13.3	0.147	445.84	0.169×10^{15}	1.218	1.103
21 47 8.5	-7 53 30.8	0.130	761.77	0.447×10^{15}	1.104	1.885
21 41 16.2	-8 23 9.2	0.129	826.61	0.702×10^{15}	1.474	2.045
15 10 8.9	+2 59 48.8	0.093	571.04	0.320×10^{15}	1.408	1.413
11 46 16.8	+11 11 1.7	0.112	397.07	0.147×10^{15}	1.337	0.983
22 58 2.6	+14 9 48.6	0.094	433.07	0.103×10^{15}	0.785	1.072
15 43 12.4	+5 52 6.2	0.106	835.13	0.932×10^{15}	1.916	2.066
11 42 17.5	+10 17 30.8	0.117	435.71	0.134×10^{15}	1.013	1.078
9 6 37.6	+10 19 5.2	0.134	762.70	0.782×10^{15}	1.928	1.887
11 44 53.8	+51 16 1.2	0.129	804.40	0.881×10^{15}	1.953	1.990
12 55 58.8	+62 8 48.5	0.105	653.23	0.303×10^{15}	1.018	1.616
0 21 7.6	-0 55 31.4	0.111	623.97	0.375×10^{15}	1.382	1.544
12 15 1.9	-2 41 25.8	0.110	347.44	0.823×10^{14}	0.978	0.860
10 29 25.1	+37 37 48.0	0.108	304.95	0.108×10^{15}	1.666	0.755
16 47 44.9	+29 10 55.2	0.134	1077.76	0.179×10^{16}	2.205	2.667
15 23 36.5	+31 1 17.4	0.074	909.39	0.120×10^{16}	2.082	2.250
22 9 56.2	-7 50 50.6	0.116	555.93	0.355×10^{15}	1.647	1.376
11 53 58.9	+9 39 29.9	0.103	766.07	0.557×10^{15}	1.360	1.896
7 59 39.4	+41 50 24.0	0.132	647.49	0.477×10^{15}	1.631	1.602
15 39 56.0	-2 11 47.8	0.150	941.81	0.129×10^{16}	2.088	2.330
11 43 45.5	+46 20 56.4	0.114	496.34	0.290×10^{15}	1.689	1.228
14 29 14.4	+33 59 23.6	0.130	919.26	0.147×10^{16}	2.500	2.275
11 48 59.9	+51 36 54.4	0.131	883.70	0.114×10^{16}	2.095	2.187
15 16 39.5	+2 47 12.8	0.111	466.11	0.173×10^{15}	1.140	1.153
14 14 12.3	+6 52 3.0	0.109	639.74	0.469×10^{15}	1.642	1.583
21 40 1.0	-8 5 53.5	0.132	709.70	0.653×10^{15}	1.860	1.756
10 49 37.8	+3 38 51.4	0.151	759.96	0.816×10^{15}	2.025	1.880
23 49 28.7	+15 14 6.7	0.114	645.35	0.361×10^{15}	1.243	1.597
11 44 1.4	-1 45 27.7	0.106	647.10	0.400×10^{15}	1.370	1.601
13 40 57.8	+3 9 53.3	0.115	483.52	0.270×10^{15}	1.653	1.196
16 7 33.4	+23 13 18.1	0.088	420.68	0.132×10^{15}	1.069	1.041
15 42 34.4	+41 49 13.1	0.141	701.91	0.616×10^{15}	1.793	1.737
14 30 33.6	+24 40 3.4	0.134	873.70	0.123×10^{16}	2.306	2.162
10 30 17.4	+41 8 28.7	0.091	483.52	0.180×10^{15}	1.105	1.196
8 54 10.1	+23 34 33.2	0.112	481.69	0.222×10^{15}	1.372	1.192
7 53 25.2	+34 16 32.5	0.139	410.75	0.151×10^{15}	1.286	1.016
8 39 16.7	+8 22 50.9	0.132	815.42	0.996×10^{15}	2.148	2.018
16 34 4.8	+40 55 59.9	0.136	591.23	0.323×10^{15}	1.326	1.463
10 31 35.7	+35 3 15.8	0.122	928.83	0.130×10^{16}	2.161	2.298
9 51 14.2	+8 16 51.6	0.142	737.42	0.729×10^{15}	1.921	1.825
10 24 37.1	+50 13 28.9	0.156	487.80	0.378×10^{15}	2.275	1.207
10 36 52.7	+44 52 35.0	0.124	763.93	0.593×10^{15}	1.457	1.890
13 56 44.8	+44 54 11.9	0.126	717.58	0.711×10^{15}	1.981	1.776
10 16 22.8	+33 38 17.5	0.129	847.43	0.110×10^{16}	2.203	2.097
14 8 6.7	+6 33 34.9	0.112	601.25	0.385×10^{15}	1.528	1.488
11 27 30.3	+0 9 19.4	0.131	517.61	0.194×10^{15}	1.039	1.281
8 44 47.3	+27 41 20.8	0.085	483.87	0.160×10^{15}	0.983	1.197
11 12 6.7	+30 40 41.9	0.074	623.97	0.326×10^{15}	1.202	1.544
21 50 36.1	-7 53 28.0	0.122	639.67	0.351×10^{15}	1.229	1.583
13 14 24.7	+62 19 45.8	0.135	580.22	0.341×10^{15}	1.452	1.436
11 43 4.0	+11 1 36.5	0.153	679.73	0.363×10^{15}	1.128	1.682
12 27 32.3	+49 28 44.0	0.119	560.16	0.261×10^{15}	1.194	1.386
10 32 9.4	+53 19 12.7	0.135	557.49	0.330×10^{15}	1.520	1.379
9 24 30.8	+7 56 56.0	0.105	423.20	0.137×10^{15}	1.096	1.047
11 4 24.8	+48 36 42.8	0.111	581.89	0.337×10^{15}	1.425	1.440
14 37 50.0	+48 36 30.6	0.122	782.47	0.769×10^{15}	1.801	1.936
8 43 33.9	+38 55 56.3	0.121	484.42	0.218×10^{15}	1.330	1.199
13 21 18.9	-0 43 43.7	0.108	627.17	0.271×10^{15}	0.987	1.552
12 1 39.0	+58 1 38.6	0.104	806.22	0.897×10^{15}	1.980	1.995

Table A.2. continued.

α (J2000.00)	δ (J2000.00)	z	σ	M_{vir}	R_{vir}	R_{200}
[h m s]	[° ' '']		[km s ⁻¹]	[h ⁻¹ M _⊙]	[h ⁻¹ Mpc]	[h ⁻¹ Mpc]
10 45 58.5	+1 26 56.0	0.105	375.80	0.143 × 10 ¹⁵	1.451	0.930
10 45 1.5	+58 5 6.0	0.116	512.04	0.226 × 10 ¹⁵	1.239	1.267
16 24 56.8	+28 33 41.4	0.145	887.74	0.724 × 10 ¹⁵	1.317	2.197
9 46 8.6	+3 46 40.8	0.119	545.97	0.317 × 10 ¹⁵	1.523	1.351
16 47 46.2	+29 10 9.5	0.134	655.71	0.600 × 10 ¹⁵	2.001	1.622
11 37 18.2	+57 8 2.8	0.117	560.11	0.201 × 10 ¹⁵	0.9acommentary20	1.386
13 48 13.1	+57 41 38.0	0.127	1090.14	0.193 × 10 ¹⁶	2.323	2.697
0 45 49.8	-0 51 1.4	0.105	567.44	0.311 × 10 ¹⁵	1.386	1.404
12 1 4.5	+15 12 35.6	0.109	529.12	0.179 × 10 ¹⁵	0.915	1.309
14 27 24.5	+55 45 1.1	0.131	713.57	0.624 × 10 ¹⁵	1.757	1.766
10 7 51.3	+62 30 2.2	0.137	560.11	0.187 × 10 ¹⁵	0.853	1.386
16 41 40.6	+22 0 54.4	0.151	850.87	0.913 × 10 ¹⁵	1.807	2.105
13 23 36.1	+4 42 40.3	0.134	794.57	0.724 × 10 ¹⁵	1.643	1.966
8 56 0.8	+48 29 10.3	0.124	668.77	0.421 × 10 ¹⁵	1.351	1.655
15 21 15.7	+32 5 12.1	0.111	827.47	0.826 × 10 ¹⁵	1.729	2.047
13 59 20.8	+49 26 51.4	0.106	553.87	0.289 × 10 ¹⁵	1.353	1.370
9 26 59.7	+54 22 36.1	0.125	673.39	0.276 × 10 ¹⁵	0.872	1.666
15 36 29.8	-1 57 48.2	0.145	716.22	0.619 × 10 ¹⁵	1.730	1.772
11 21 35.4	+35 23 24.7	0.103	591.23	0.395 × 10 ¹⁵	1.619	1.463
11 48 20.4	+10 21 8.3	0.113	999.27	0.158 × 10 ¹⁶	2.269	2.473
10 48 8.8	+31 28 31.1	0.115	623.88	0.302 × 10 ¹⁵	1.112	1.544
14 23 49.9	+6 14 32.3	0.113	463.77	0.224 × 10 ¹⁵	1.495	1.148
14 48 18.4	+3 31 44.4	0.124	741.07	0.522 × 10 ¹⁵	1.362	1.834
8 1 7.0	+17 58 45.1	0.144	454.09	0.109 × 10 ¹⁵	0.756	1.124
11 13 33.7	+37 22 27.8	0.102	556.72	0.300 × 10 ¹⁵	1.386	1.378
9 40 30.1	+2 28 35.4	0.151	865.54	0.813 × 10 ¹⁵	1.556	2.142
9 1 18.4	+58 16 8.0	0.097	839.35	0.547 × 10 ¹⁵	1.113	2.077
14 42 58.5	+55 10 55.2	0.105	435.71	0.111 × 10 ¹⁵	0.840	1.078
8 44 36.5	+29 21 12.6	0.099	505.37	0.171 × 10 ¹⁵	0.960	1.250
10 38 1.8	+41 46 25.7	0.124	567.73	0.289 × 10 ¹⁵	1.285	1.405
14 52 33.6	+50 55 22.1	0.131	560.11	0.313 × 10 ¹⁵	1.430	1.386
14 6 25.0	+6 35 3.1	0.113	477.41	0.239 × 10 ¹⁵	1.501	1.181
12 16 49.1	-3 7 55.2	0.111	435.64	0.134 × 10 ¹⁵	1.012	1.078
23 6 18.9	+14 9 40.7	0.112	475.07	0.236 × 10 ¹⁵	1.500	1.175
1 42 25.6	-10 16 11.6	0.112	507.75	0.250 × 10 ¹⁵	1.391	1.256
14 17 54.2	+43 23 17.2	0.105	430.73	0.168 × 10 ¹⁵	1.296	1.066
13 23 48.6	+1 6 48.2	0.108	668.18	0.369 × 10 ¹⁵	1.187	1.653
8 44 21.1	+51 24 21.2	0.097	496.13	0.186 × 10 ¹⁵	1.081	1.228
11 51 10.7	-3 1 41.2	0.091	212.72	0.268 × 10 ¹⁴	0.850	0.526
10 19 35.7	+14 2 26.5	0.146	631.06	0.544 × 10 ¹⁵	1.959	1.561
12 13 58.5	+63 13 16.0	0.133	541.44	0.170 × 10 ¹⁵	0.831	1.340
16 20 8.2	+42 30 2.9	0.135	658.63	0.524 × 10 ¹⁵	1.732	1.630
10 17 17.7	+8 40 57.7	0.104	522.25	0.215 × 10 ¹⁵	1.131	1.292
11 37 36.7	+32 26 40.6	0.103	510.52	0.174 × 10 ¹⁵	0.959	1.263
8 28 0.9	+28 15 51.8	0.093	418.11	0.136 × 10 ¹⁵	1.119	1.035
9 16 26.7	+5 55 15.2	0.134	754.05	0.637 × 10 ¹⁵	1.606	1.866
10 9 35.2	+7 9 50.8	0.099	425.58	0.131 × 10 ¹⁵	1.038	1.053
11 40 9.3	+32 23 20.4	0.131	818.31	0.852 × 10 ¹⁵	1.825	2.025
23 47 55.1	+14 54 52.2	0.105	424.17	0.205 × 10 ¹⁵	1.630	1.050
10 28 28.7	+9 38 58.6	0.106	581.90	0.382 × 10 ¹⁵	1.619	1.440
0 5 21.1	+15 58 4.8	0.117	541.07	0.430 × 10 ¹⁵	2.106	1.339
9 6 49.9	+4 46 45.8	0.126	727.16	0.475 × 10 ¹⁵	1.288	1.799
10 11 58.3	+33 34 15.2	0.127	631.29	0.349 × 10 ¹⁵	1.255	1.562
9 39 9.5	+37 40 1.6	0.148	835.21	0.588 × 10 ¹⁵	1.208	2.067
10 43 52.0	+1 3 42.1	0.117	419.59	0.140 × 10 ¹⁵	1.137	1.038
13 11 22.6	+48 30 45.4	0.140	807.27	0.970 × 10 ¹⁵	2.134	1.997
3 5 59.3	-0 9 59.4	0.110	623.76	0.256 × 10 ¹⁵	0.944	1.543
12 10 52.2	+15 55 35.0	0.107	553.89	0.262 × 10 ¹⁵	1.227	1.371
12 19 9.3	+63 31 42.2	0.107	611.17	0.405 × 10 ¹⁵	1.554	1.512

Table A.2. continued.

α (J2000.00)	δ (J2000.00)	z	σ	M_{vir}	R_{vir}	R_{200}
[h m s]	[° ′ ″]		[km s ⁻¹]	[$h^{-1} M_{\odot}$]	[h^{-1} Mpc]	[h^{-1} Mpc]
10 27 26.5	+37 52 37.6	0.107	403.63	0.163×10^{15}	1.435	0.999
9 50 53.3	+28 48 15.5	0.113	810.78	0.837×10^{15}	1.827	2.006
12 11 9.8	+6 10 49.8	0.138	559.20	0.240×10^{15}	1.101	1.384
10 25 0.7	+49 51 33.5	0.135	1120.42	0.153×10^{16}	1.743	2.772
14 33 39.1	+61 22 3.4	0.113	618.08	0.446×10^{15}	1.675	1.529
11 41 15.1	+10 43 15.6	0.105	636.26	0.436×10^{15}	1.545	1.574
9 53 52.6	+12 15 55.4	0.129	521.13	0.286×10^{15}	1.508	1.289
10 28 45.1	+37 52 38.3	0.107	541.02	0.421×10^{15}	2.062	1.339
10 10 45.3	+33 43 3.7	0.135	664.31	0.685×10^{15}	2.224	1.644
10 21 16.9	+12 13 0.1	0.129	537.06	0.341×10^{15}	1.695	1.329
9 46 38.1	+29 42 2.2	0.112	253.32	0.473×10^{14}	1.057	0.627
13 2 59.1	+51 18 56.5	0.121	554.46	0.284×10^{15}	1.323	1.372
1 19 16.5	+14 42 31.0	0.129	525.18	0.339×10^{15}	1.760	1.299
8 25 48.4	+56 0 48.2	0.138	648.50	0.350×10^{15}	1.195	1.605
13 48 19.9	+57 45 34.6	0.127	541.44	0.323×10^{15}	1.582	1.340
22 56 28.3	-0 32 53.9	0.110	430.58	0.123×10^{15}	0.948	1.065
7 59 41.8	+28 46 55.6	0.139	503.43	0.177×10^{15}	0.999	1.246
14 32 22.8	+47 6 38.2	0.109	311.13	0.698×10^{14}	1.034	0.770
11 15 16.5	+53 42 42.5	0.105	903.25	0.106×10^{16}	1.867	2.235
23 14 58.7	+14 5 24.4	0.083	517.16	0.212×10^{15}	1.135	1.280
10 11 11.4	+8 41 31.9	0.097	385.05	0.140×10^{15}	1.357	0.953
15 27 0.2	+29 41 33.0	0.113	689.54	0.512×10^{15}	1.543	1.706
15 51 37.4	+45 33 16.2	0.124	693.77	0.441×10^{15}	1.314	1.717
11 19 49.4	+55 15 37.8	0.106	537.54	0.251×10^{15}	1.245	1.330
8 6 33.0	+29 28 55.6	0.128	458.29	0.204×10^{15}	1.390	1.134
8 20 55.8	+7 52 12.7	0.110	558.19	0.287×10^{15}	1.321	1.381
14 14 9.8	-0 8 26.9	0.139	1091.89	0.190×10^{16}	2.280	2.702
11 21 53.8	+0 41 55.0	0.102	654.86	0.422×10^{15}	1.410	1.620
11 20 19.8	+47 4 54.5	0.112	572.08	0.359×10^{15}	1.570	1.416
10 48 58.7	+54 53 22.9	0.145	672.72	0.557×10^{15}	1.765	1.665
14 59 8.5	+47 19 43.0	0.089	677.50	0.660×10^{15}	2.062	1.676
10 27 49.7	+3 40 43.7	0.074	819.40	0.960×10^{15}	2.051	2.027
21 29 58.2	-0 19 47.6	0.135	323.62	0.126×10^{15}	1.721	0.801